

Cave airflow patterns control calcite dissolution rates within a cave stream: Blowing Springs Cave, Arkansas, USA

Matthew D. Covington^{a,b}, Katherine J. Knierim^c, Holly A. Young^a, Josue Rodriguez^a, Hannah G. Gnoza^a

^a*Department of Geosciences, University of Arkansas, Fayetteville, Arkansas, USA*

^b*Karst Research Institute, ZRC SAZU, Slovenia*

^c*United States Geological Survey*

Abstract

Erosion rates within streams vary dramatically over time, as differences in discharge and sediment load enhance or inhibit erosion processes. Within cave streams, and other bedrock channels incising soluble rocks, changes in water chemistry are an important factor in determining how erosion rates will vary in both time and space. Prior studies within surface streams, springs, and caves suggest that variation in dissolved CO₂ is the strongest control on variation in calcite dissolution rates. However, the controls on CO₂ variation remain poorly quantified. Limited data suggest that ventilation of karst systems can substantially influence dissolved CO₂ within karst conduits. However, the interactions among cave ventilation, air-water CO₂ exchange, and dissolution dynamics have not been studied in detail. Here we analyze three years of time series measurements of dissolved and gaseous CO₂, cave airflow velocity, and specific conductance from Blowing Springs Cave, Arkansas. We use these time series to estimate continuous calcite dissolution rates and quantify the correlations between those rates and potential physical and chemical drivers. We find that chimney effect airflow creates temperature-driven switches in airflow direction, and that the resulting seasonal changes in airflow regulate both gaseous and dissolved CO₂ within the cave. As in previous studies, partial pressure of CO₂ (pCO₂) is the strongest chemical control of dissolution rate variability. However, we also show that cave airflow direction, rather than stream discharge, is the strongest physical driver of changes in dissolution rate, contrary to the typical situation in surface channel erosion where floods largely determine the timing and extent

of geomorphic work. At the study site, chemical erosion is typically active in the summer, during periods of cave downdraft (airflow from upper to lower entrances), and inactive in the winter, during updraft (airflow from lower to upper entrances). Storms provide only minor perturbations to this overall pattern. We also find that airflow direction modulates dissolution rate variation during storms, with higher storm variability during updraft than during downdraft. Finally, we compare our results with the limited set of other studies that have examined dissolution rate variation within cave streams and draw an initial hypothesis that evolution of cave ventilation patterns strongly impacts how dissolution rate dynamics evolve over the lifetime of karst conduits.

Keywords:

karst, bedrock channel, speleogenesis, carbon dioxide, dissolution

1. Introduction

2 The variation in geomorphic rates has an important influence on the
3 relationship between erosional processes and the landforms that they pro-
4 duce (Wolman and Miller, 1960). Whereas concepts of the magnitude and
5 frequency of geomorphic work have long been explored in the study of pro-
6 cesses on Earth’s surface, fewer studies have examined the variability in rates
7 of cave development or the factors that control this variation (Groves and
8 Meiman, 2005). Cave passages are typically developed by subsurface streams
9 incising through bedrock. Since many cave streams carry substantial sedi-
10 ment loads (Farrant and Smart, 2011), mechanical erosion processes, as occur
11 within surface bedrock channels (Whipple et al., 2000), undoubtedly are ac-
12 tive within these streams. However, most caves develop in karst settings,
13 within highly soluble rocks, where chemical dissolution of the rock is an im-
14 portant driver of channel development and evolution (Ford and Williams,
15 2007; Palmer, 2007a).

16 A number of studies have measured solute export from basins and used
17 these data to examine how rates of chemical denudation vary with discharge
18 (Wolman and Miller, 1960; Gunn, 1982; Schmidt, 1985; Goudie and Viles,
19 1999). These studies conclude that low to moderate flows produce an impor-
20 tant percentage of the overall chemical geomorphic work at the basin scale.
21 However, rates of channel incision by dissolution and basin wide chemical de-
22 nudation do not in general display the same relationship to discharge. Groves

23 and Meiman (2005) show that, in the Logsdon River passage of Mammoth
24 Cave, Kentucky, conduit wall dissolution rates are a strong function of dis-
25 charge, with 87% of the work being done during high discharges that occur
26 less than 5% of the time. In contrast, they find that solute export is im-
27 portant across a range of discharges, with only 38% of the export occurring
28 during the highest discharge class. Palmer (2007b) finds a similar relationship
29 between discharge and calcite dissolution rate in McFail’s Cave, New York.
30 Analysis of water chemistry data from streams across the United States sug-
31 gests that variability in calcite dissolution rates at most sites is more strongly
32 correlated with variability in dissolved CO₂ than with discharge, and that in-
33 channel dissolution rates are often much higher than estimates of basin wide
34 denudation rates (Covington et al., 2015). Covington and Vaughn (2019)
35 showed that seasonal variability in CO₂ is the primary driver for variation in
36 calcite dissolution rates at a pair of karst underflow-overflow springs. Addi-
37 tionally, they hypothesize that, during low flows, ventilation within the con-
38 duct feeding the overflow spring drives a reduction in CO₂ and, consequently,
39 dissolution rates. In general, previous investigators have argued that cave
40 ventilation, which often occurs in the later stages of cave development, may
41 reduce the rates of chemical erosion within cave streams as caves becomes
42 more mature (Palmer, 2007b).

43 While it is clear that both floods and CO₂ dynamics are important drivers
44 of dissolution rate variability within cave streams, there are relatively few
45 cave sites where dissolution rate variability has been quantified (Groves and
46 Meiman, 2005; Palmer, 2007b; Covington and Vaughn, 2019). This lack of
47 data limits the ability to generalize about the controls on calcite dissolution
48 rate variability. Here, we analyze water chemistry data in a cave stream in the
49 Ozark Plateaus of Arkansas to explore potential controls of dissolution rate
50 variability. We use recently developed techniques for direct, high temporal
51 resolution measurements of dissolved CO₂ (Johnson et al., 2010), combined
52 with time series of specific conductance (SpC), to enable estimates of calcite
53 dissolution rates over a three year period. These measurements are com-
54 plemented by simultaneous measurements of cave air CO₂ and cave airflow
55 velocity. This enables us to explore interactions between cave atmosphere
56 dynamics and cave stream chemistry.

57 **2. Description of field site**

58 Blowing Springs Cave is located in Bella Vista, Arkansas, within the
59 Springfield Plateau region of the Ozark Plateaus (Figure 1). The cave is
60 developed in the cherty Mississippian Boone Limestone primarily within the
61 St. Joe Limestone Member (McFarland, 1998). Because of a high concentra-
62 tion of chert and clay impurities, the Boone Limestone develops a mantled
63 karst, where a thick regolith composed of chert and clay covers the karst
64 surface (Brahana, 2011). Within the region surrounding the cave, the Boone
65 Limestone spans the topography from valley floors to ridges. The cave, there-
66 fore, is autogenically recharged through a regolith cover. Because of the re-
67 golith cover, the region contains few obvious surface karst features, such as
68 sinkholes, though most of the valleys located in the recharge area are dry ex-
69 cept during periods of intense precipitation. The land cover in the recharge
70 area is a mixture of deciduous forest and low intensity residential. The region
71 has a temperate continental climate with a mean annual air temperature of
72 approximately 15°C (Adamski et al., 1995) and a mean annual precipitation
73 of about 114 centimeters per year (cm/yr) (Pugh and Westerman, 2014).

74 Blowing Springs Cave contains 2,397 meters (m) of mapped cave passage
75 and consists of a dendritic stream network (Figure 1). Water enters the
76 main cave stream through a number of small infeeding channels and through
77 many percolating fractures within the cave ceiling, though the largest source
78 of discharge to the cave stream is the upstream sump. Many of the cave
79 passages are oriented along an orthogonal set of NE-SW and NW-SE trending
80 fractures. The only known entrance of the cave is at the spring, and, as
81 the name suggests, the cave exhibits strong airflow, with air blowing out of
82 the spring entrance during times of warm outside temperatures. The spring
83 emerges near the elevation of the local base-level stream, which is Little Sugar
84 Creek.

85 **3. Methods**

86 *3.1. Collection of time series data*

87 Time series data of water quality and cave atmospheric parameters were
88 collected at a site located approximately 150 m inside the cave entrance,
89 which is labeled as Cave Measurement Station in Figure 1. Cave airflow
90 velocity, cave air barometric pressure, and CO₂ concentrations in the cave
91 air and water were logged on a Campbell Scientific CR850 datalogger. Cave

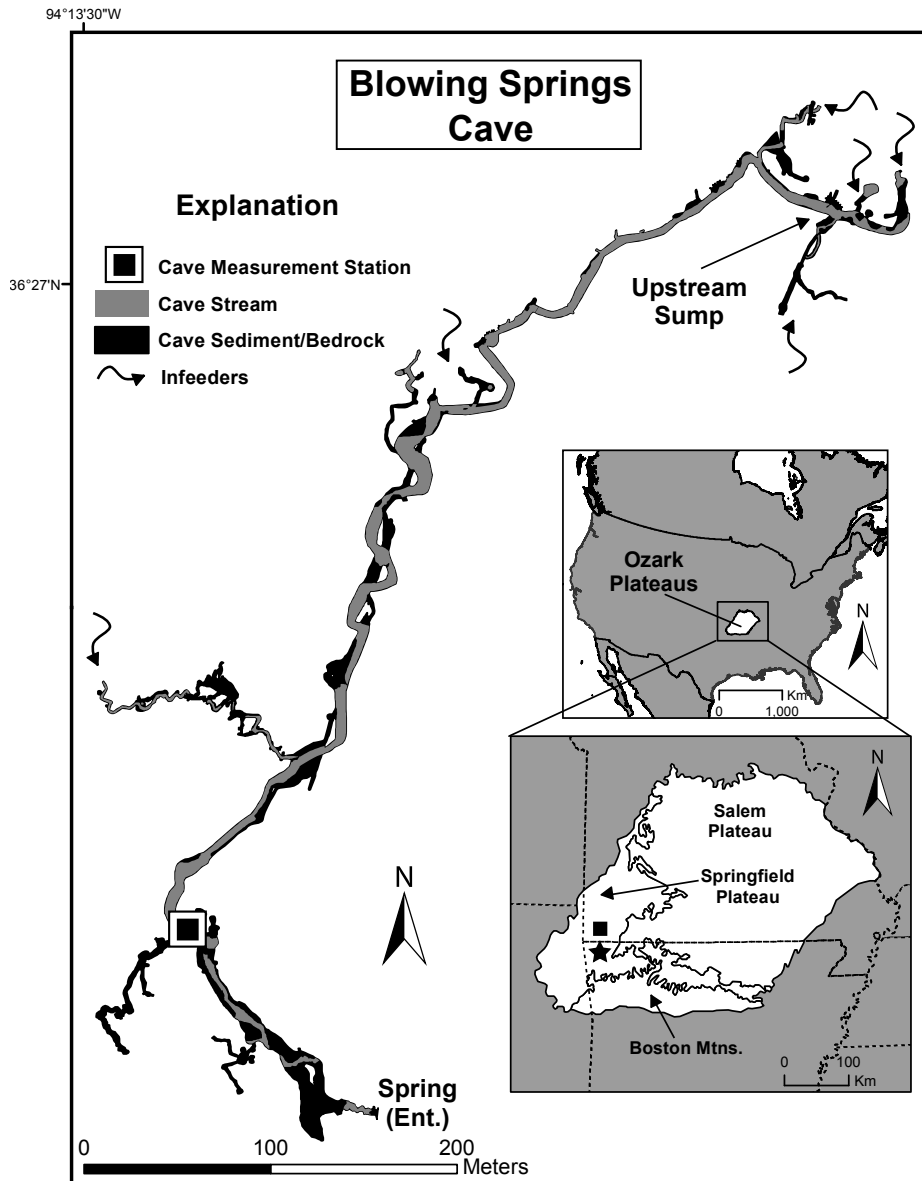


Figure 1: Location of Blowing Springs Cave (star) and map of the cave depicting the entrance, measurement location, stream, and upstream sump. Within the inset, the square indicates the location of the USGS gauge on Little Sugar Creek (USGS-07188838). Modified from Knierim et al. (2017). Original cave map and survey data from Covington (2007).

92 airflow velocity and direction were measured using a Campbell Scientific
93 WINDSONIC1 2D ultrasonic anemometer (resolution 0.01 m/s; accuracy
94 $\pm 2\%$ at 12 m/s; directional accuracy $\pm 3^\circ$). Barometric pressure was mea-
95 sured using a Campbell Scientific CS100 sensor (accuracy ± 0.5 hPa). CO₂
96 concentrations in the air and water were measured using Vaisala GMM220
97 CO₂ transmitters with a range of 0 to 5000 parts per million (ppm) (accu-
98 racy $\pm 1.5\%$ of range $\pm 2\%$ of reading). The CO₂ sensors were protected from
99 moisture with a waterproof breathable membrane (PTFE) as described in
100 Johnson et al. (2010). One sensor was placed in the cave air, and the other
101 was submerged in the cave stream to enable direct measurement of the par-
102 tial pressure of CO₂ (pCO₂) of the water. This setup provides a more reliable
103 means of recording pCO₂ than continuous measurement of pH, as the CO₂
104 sensors exhibit much less drift over time than pH electrodes (Johnson et al.,
105 2010; Covington and Vaughn, 2019). For the CO₂ sensors, a warm-up pe-
106 riod of 15 minutes was used before a measurement was taken. This warm-up
107 period allowed thermal equilibration of the sensor and helped to drive any
108 moisture out of the sensor optics. We found that this warm-up period was
109 crucial, as substantial instrument drift occurred within the first few minutes
110 of power-up. Measured values of pCO₂ were not adjusted with water depth as
111 described by (Johnson et al., 2010), because subsequent theoretical analysis
112 and experiments have shown that this adjustment is incorrect (Blackstock
113 et al., 2019). CO₂ readings were taken once an hour to conserve power,
114 whereas other parameters recorded on the CR850 were read on a one-minute
115 interval.

116 The specific conductance (SpC) and temperature of the cave stream were
117 measured at the same site as CO₂ on a time interval of 5 minutes using
118 an Onset HOBO U24-001 freshwater conductivity logger with an accuracy
119 of 3% or 5 microsiemens per centimeter ($\mu\text{S}/\text{cm}$). Outside of the cave, air
120 temperature and relative humidity were measured at a 5 minute interval
121 using an Onset HOBO U23-001 temperature (accuracy $\pm 0.21^\circ\text{C}$) and relative
122 humidity (accuracy $\pm 2.5\%$) logger that was mounted onto a tree. To provide
123 a proxy for stable cave temperature, we deployed an Onset HOBO U20L-04
124 pressure and temperature logger in the cave air approximately 400 m inside
125 the cave (accuracy $\pm 0.44^\circ\text{C}$). Unless specified otherwise, all data presented
126 here are hourly averages, to align with the frequency of CO₂ measurements.

127 The site within the cave was visited roughly every four weeks, which was
128 the approximate duration of the battery power supply (two 12-volt, 20 Amp-
129 hour lithium-ion batteries). During each site visit, batteries were changed,

130 data downloaded, and quality control spot measurements were made of spe-
131 cific conductance, water temperature, and CO₂ concentrations in the air and
132 water. To make spot measurements of CO₂ a portable Vaisala GMM220 was
133 used that was connected to a battery and data logger. Spot measurements of
134 CO₂ in the water required a roughly 30-minute equilibration period for gas
135 concentrations to exchange across the PTFE membrane.

136 Whereas a partial record of stage and estimated discharge is available at
137 the spring, frequent human disturbances of the stream channel near the weir
138 (the site is located in a park) reduce the quality of the available dataset.
139 Rather than using this corrupted record, we employ an estimation of dis-
140 charge at Blowing Springs Cave developed by Knierim et al. (2015b) using the
141 nearby USGS streamflow-gaging station on Little Sugar Creek (07188838 Lit-
142 tle Sugar Creek near Pineville, Missouri) with data available from the USGS
143 National Water Information System (U.S. Geological Survey, 2020) (daily
144 streamflow accessed May 19, 2020, at [https://waterdata.usgs.gov/mo/
145 nwis/dv/?site_no=07188838&agency_cd=USGS](https://waterdata.usgs.gov/mo/nwis/dv/?site_no=07188838&agency_cd=USGS)).

146 They found that a linear regression of

$$Q_{BS} = 0.0066Q_{LS} + 0.0023, \quad (1)$$

147 where Q_{BS} is discharge at Blowing Spring and Q_{LS} is discharge at Little
148 Sugar Creek (discharge units are m³/s), provided a reasonable approxima-
149 tion of discharge at Blowing Springs Cave over a 15-month study period.
150 Whereas this relationship often underestimates peak flows of floods, and can
151 also underestimate baseflow, it provides a reasonable proxy for the discharge
152 dynamics at the study site. Discharge data used here are daily averages
153 and are used only to indicate the occurrence and frequency of high and low
154 flow periods to examine how dissolution rate varies with flow. The precise
155 magnitudes of discharge are not necessary for interpreting our data.

156 3.2. Calculation of dissolution rates

157 In order to calculate dissolution rates from available kinetic rate equa-
158 tions, we need values for the dissolved Ca concentration and the pCO₂. While
159 we measure pCO₂ directly, Ca concentrations are estimated from SpC time
160 series collected at the site, as has also been done in prior studies of dissolution
161 rate dynamics within karst systems (Groves and Meiman, 2005; Covington
162 and Vaughn, 2019) and is appropriate where water is predominantly Ca-
163 HCO₃ type. To estimate Ca, we use a linear regression on available SpC and

164 Ca data ($n = 109$) from a prior study at Blowing Springs Cave (Knierim
165 et al., 2017). This enables estimation of Ca concentrations from the SpC
166 within about 15–20% using a relationship of $[Ca] = 0.175 \times SpC - 2.51$,
167 where $[Ca]$ is concentration in mg/L.

168 To calculate dissolution rates from $[Ca]$ and pCO_2 time series, we use two
169 available calcite kinetic equations, which we refer to as the PWP (Plummer
170 et al., 1978) and Palmer equations (Palmer, 1991). Both equations are de-
171 rived from the same experimental dataset, but the Palmer equation is a direct
172 fit to the data, whereas the PWP equation incorporates a more mechanistic
173 approach to parameter estimation. The Palmer equations generate a closer fit
174 to the observed dissolution rates near saturation and also provide parameter
175 values for impure calcite, which is more appropriate for limestone. Coving-
176 ton and Vaughn (2019) found that the Palmer equation provided much closer
177 estimates of mass loss rates of limestone tablets deployed in the field, and
178 therefore, it is likely that these rates are more accurate in natural settings.

179 The PWP equation also produces negative rates, which might suggest
180 calcite precipitation. However, calcite precipitation normally does not occur
181 until waters are highly supersaturated, therefore negative PWP rates are not
182 necessarily indicative of precipitation. In time series of dissolution rates, we
183 show both the PWP and Palmer equations. However, when studying sensitiv-
184 ity of rates to various potential controls, it is helpful to have a broader range
185 of values, including a range of negative values that represent different extents
186 of supersaturation. Therefore, we use PWP rates to explore controls on vari-
187 ability, even though the magnitude of the rates is likely too high (Covington
188 and Vaughn, 2019). Rates predicted by both equations typically vary mono-
189 tonically with one another. Both dissolution rate equations were calculated
190 using algorithms in the *Olm* Python package v0.35 (Covington et al., 2015),
191 which is available on *Github* (<https://doi.org/10.5281/zenodo.3836604>).

192 4. Results

193 4.1. Large scale patterns in the time series data

194 The water chemistry and cave atmosphere parameters were recorded over
195 a period of approximately three years (Oct. 2014-Jan. 2018). Several regular
196 patterns emerge from the data. CO_2 concentrations in air and water range
197 between near atmospheric concentration (≈ 500 ppm) to above 5000 ppm
198 (Figure 2a). For a few short periods, pCO_2 in the water exceeded the mea-
199 surement range of the sensor deployed (≈ 5500 ppm). Concentrations in the

200 water almost always exceeded those in the air. Both dissolved and gaseous
201 CO₂ concentrations within the cave showed seasonal patterns, with higher
202 concentrations in summer and lower concentrations during winter. Gaseous
203 CO₂ within the cave dropped near atmospheric values for much of the winter.
204 Dissolved CO₂ often exhibited spikes to higher values associated with high
205 discharge events. Gaseous CO₂ displayed strong diurnal variability during
206 certain periods, particularly during the spring and fall. These periods of
207 variability are associated with times when outside air temperatures are near
208 those of the cave air temperature, which is approximately the mean surface
209 air temperature (Badino, 2010).

210 Cave airflow velocity also had a seasonal pattern with outward (positive)
211 airflow during warm periods and inward (negative) airflow during cold pe-
212 riods (Figure 2b). There was strong diurnal variability in airflow velocity,
213 particularly during spring and fall periods, with some days exhibiting both
214 inward and outward airflow at different times of day. Again, these periods of
215 high variability are times when outside temperatures are near the tempera-
216 ture of the cave atmosphere.

217 Specific conductance displayed a range from 65 to 265 $\mu\text{S}/\text{cm}$. Variability
218 in SpC was more strongly related to discharge than to season (Figures 2c,d).
219 SpC was high during periods of low flow and low during periods of high flow,
220 particularly flood events. All records display gaps that are associated with
221 sensor or power failures. However, the SpC record is the least complete, with
222 a large number of gaps resulting from sensor failure, damage during storms,
223 or download failure, which lead to memory filling on the datalogger before the
224 next opportunity to download. As can be seen visually in Figures 2c,d, there
225 is a strong correlation between specific conductance and stream discharge
226 (Q). The relationship between these parameters is explicitly displayed in
227 Figure 3 along with a 4th-order polynomial regression between $\log(Q)$ and
228 specific conductance given by

$$\text{SpC} = Ax^4 + Bx^3 + Cx^2 + Dx + E, \quad (2)$$

229 where $x = \log(Q)$, $A = -25.46$, $B = 218.9$, $C = -649.8$, $D = 704.9$, and
230 $E = 10.42$. The coefficients were determined using the *polyfit()* function from
231 the *NumPy* package in Python. Because of the large number of gaps, and
232 the strong relationship between discharge and SpC, the daily estimated SpC
233 using this regression with discharge is shown in Figure 2c. The root-mean-
234 squared error in estimated SpC is 14.9 $\mu\text{S}/\text{cm}$. The valid discharge range

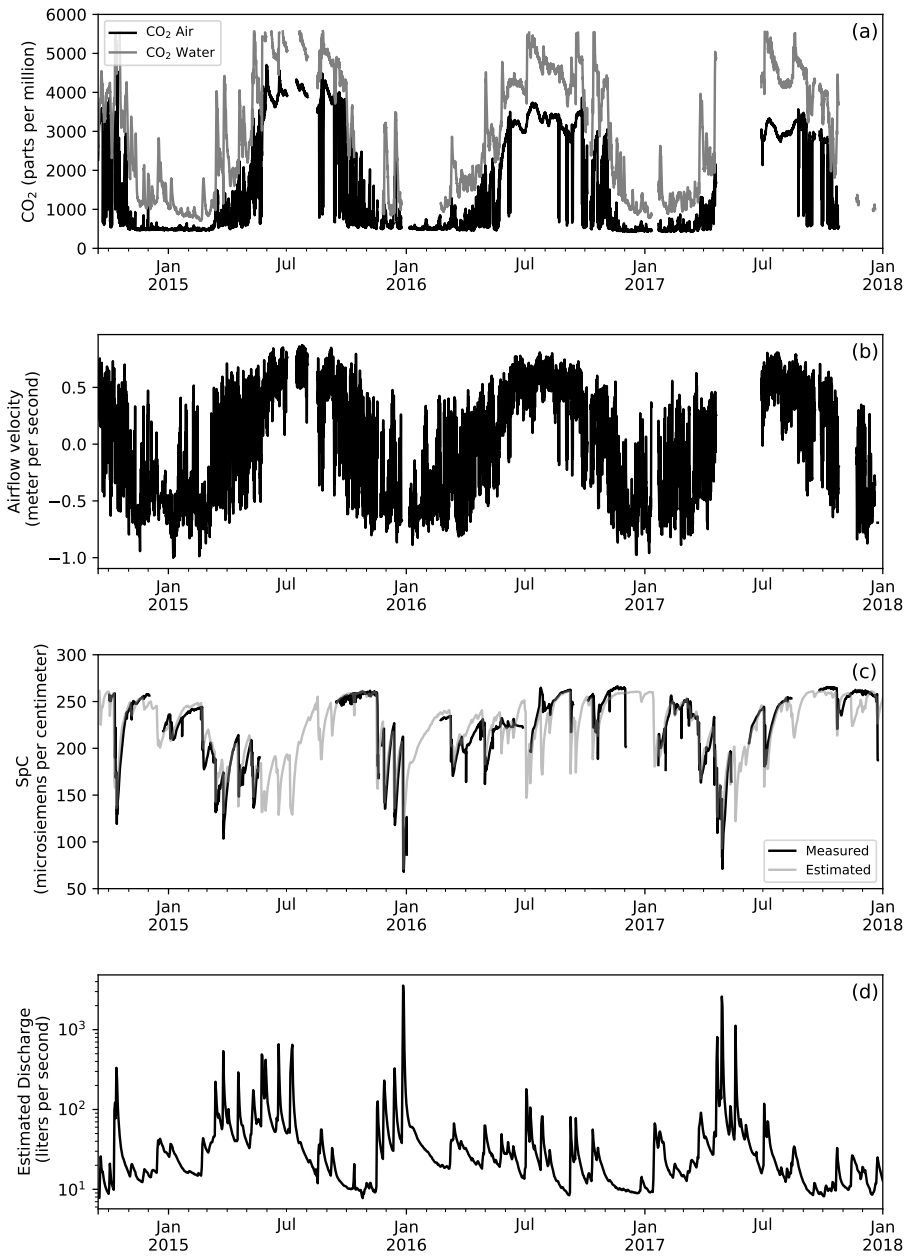


Figure 2: Time series data for the entire study period: (a) CO₂ concentrations in the air and water, (b) cave airflow velocity (positive values indicate the cave is blowing out), (c) specific conductance of the cave stream (black) and an estimated daily specific conductance using a regression to stream discharge (gray), and (d) estimated discharge of the cave calculated from discharge at Little Sugar Creek using regression from Knierim et al. (2015b).

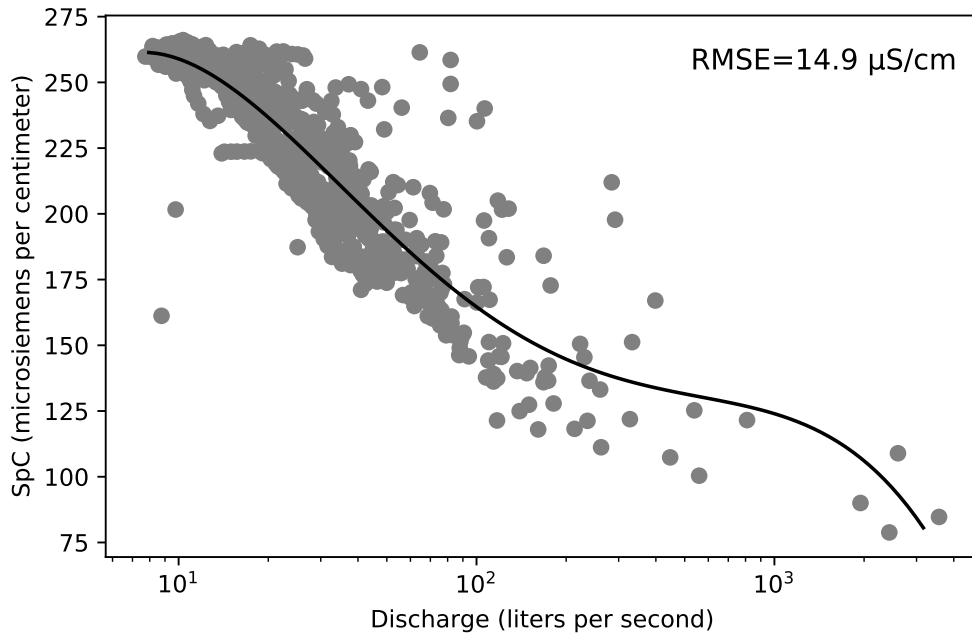


Figure 3: Relationship between specific conductance and discharge shown along with polynomial regression (Equation 2) used for estimating specific conductance during periods of missing record (RMSE=root-mean-squared error).

235 for the fit is from approximately 10 L/s to 2000 L/s. The results do not
 236 depend on filling these gaps in the record, but the estimated curve does aid
 237 in visualizing the long-term patterns.

238 *4.2. Relationship between cave airflow and external air temperature*

239 The seasonal and diurnal patterns in cave airflow velocity suggest a re-
 240 lationship between outside air temperature and cave airflow, as would be
 241 expected in the case of chimney effect airflow (Wigley and Brown, 1976;
 242 Luetscher et al., 2008; Badino, 2010; Covington and Perne, 2015). Chimney
 243 effect airflow is an airflow mechanism driven by density contrasts between
 244 the cave air and outside air and occurs within cave systems with more than
 245 one opening to the outside. During periods of warm outside temperatures,
 246 cave air is more dense than outside air and it is therefore pushed from upper
 247 entrances to lower entrances. During cold outside temperatures cave air is

248 less dense than outside air and rises from lower entrances to upper entrances.
 249 Note that such airflow does not require human-sized entrances or large el-
 250 evation differences. Millimeter-scale fracture apertures and decimeters of
 251 elevation difference are sufficient (Covington, 2016).

252 The pressure difference, ΔP , that drives chimney effect airflow can be
 253 approximated using (cf. Badino (2010))

$$\Delta P = \rho_{\text{in}} g h \frac{\Delta T}{T_{\text{ext}}}, \quad (3)$$

254 where ρ_{in} is the density of the air inside the cave, g is Earth’s gravitational
 255 acceleration, h is the height difference between the two entrances, ΔT is the
 256 difference between cave and external temperature, and T_{ext} is the external
 257 air temperature in Kelvin. Chimney effect airflow is typically turbulent, and
 258 therefore the Darcy–Weisbach equation for flow of fluid in a pipe provides a
 259 reasonable approximation (Luetscher and Jeannin, 2004) for airflow velocity,
 260 V , with

$$V = \sqrt{\frac{2D_{\text{H}}\Delta P}{\rho_{\text{in}}fL}}, \quad (4)$$

261 where D_{H} is the hydraulic diameter of the flow path, f is the Darcy-Weisbach
 262 friction factor, and L is the length of the flow path. Combining these two
 263 equations, leads to

$$V = \sqrt{\frac{2D_{\text{H}}gh\Delta T}{fLT_{\text{ext}}}}, \quad (5)$$

264 where one can see that the airflow velocity is predicted to scale with the
 265 square root of the temperature difference between outside and cave air. To
 266 test the plausibility of chimney effect airflow as the primary mechanism be-
 267 hind the observed airflow in Blowing Springs Cave, airflow velocity is plotted
 268 against the temperature difference between inside and outside air, and a
 269 square root relationship is fit to the data (Figure 4). Not only is there a
 270 strong relationship between temperature difference and cave airflow velocity,
 271 but the shape of the relationship is closely matched by a square root function,
 272 $V = R\Delta T^{1/2}$, where the best fit value of the resistance factor $R = 0.18$.

273 There are no known human-sized upper entrances to Blowing Springs
 274 Cave. However, we can use knowledge of the cave system to estimate ap-
 275 propriate values of unknown parameters in Equation 5, using $L = 1000$ m,
 276 which is the approximate distance from the entrance to the upstream sump,

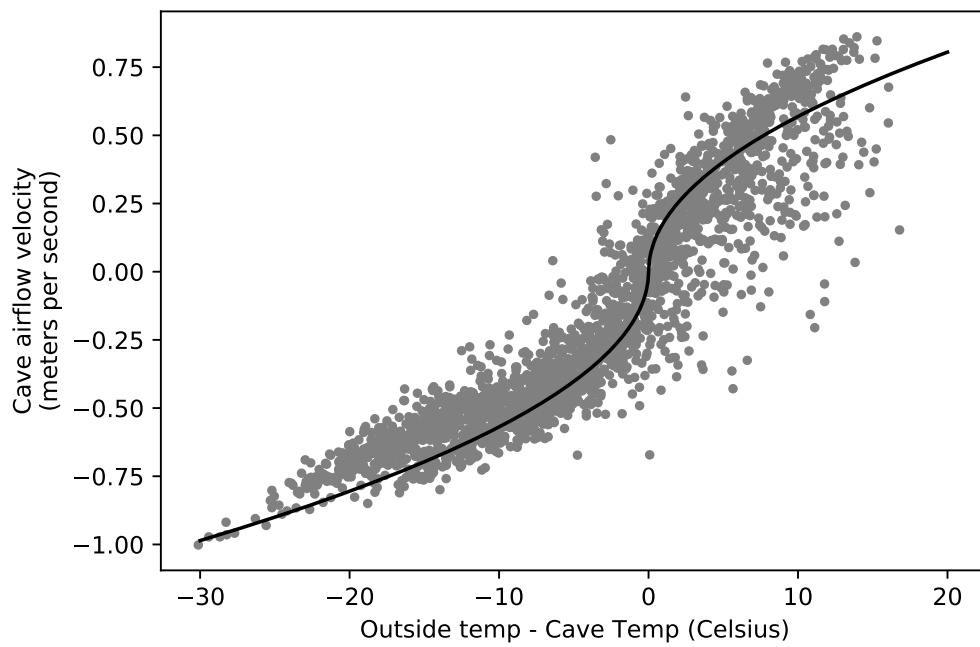


Figure 4: Relationship between airflow velocity and temperature difference between outside air and cave air, with a fitting function $V = R\Delta T^{1/2}$, with the resistance factor set to $R = 0.18$.

277 and $h = 25$ m, which is the approximate elevation difference between the
278 spring entrance and the valleys feeding the cave that are likely to hold upper
279 entrances. Using values of $g = 9.8 \text{ m/s}^2$ and $f = 0.05$, which is a typical
280 value for a rough pipe and high Reynolds Number (Larock et al., 2000), we
281 can estimate that the hydraulic diameter would have to be approximately
282 equal to a meter in order to produce the observed value of R . Though di-
283 ameters of the mapped portion of the cave are highly variable (Figure 1),
284 with values reaching up to 5–10 meters within larger rooms, a diameter of
285 one meter is roughly consistent with observed diameters in much of the cave.
286 The untraversable upper portions of the flow paths must also be substantially
287 smaller, because they are too small for a human to enter.

288 To make the link between airflow direction and the chimney effect mech-
289 anism explicit in our further discussion, from this point on we will refer to
290 cave airflow direction as either “updraft” or “downdraft” (Figure 5). Updraft
291 occurs during periods when the cave air is less dense than outside air (e.g.
292 winter) and air flows from lower to upper entrances (inward). Downdraft
293 occurs when the cave air is denser than outside air (e.g. summer) and air
294 flows from upper to lower entrances (outward). Because the airflow velocity
295 was measured near a lower entrance, updraft corresponds to inward airflow
296 (negative velocity), and downdraft corresponds to outward airflow (positive
297 velocity).

298 *4.3. Relationship between airflow velocity and CO₂*

299 The seasonal patterns in cave airflow and CO₂ in the air and water are well
300 aligned (Figure 2). Additionally, there are strong relationships between CO₂
301 and cave airflow on short timescales (Figure 6). During periods of diurnal
302 airflow reversals, CO₂ in the cave air also shows daily peaks and troughs.
303 When airflow direction switches from downdraft to updraft, cave air CO₂
304 drops suddenly to concentrations near atmospheric (~ 500 ppm), as outside
305 air is quickly brought to the location of the sensor. When airflow switches
306 from updraft to downdraft, cave air CO₂ rises somewhat more slowly, likely
307 as a result of mixing of high and low CO₂ air within the cave atmosphere.
308 Dissolved CO₂ within the cave stream does not respond as rapidly to airflow
309 reversals as the cave air. However, the cave stream CO₂ does have a muted
310 response that has a lag of a few days (Figure 6).

311 Dissolved and gaseous CO₂ both display statistically significant corre-
312 lations (p-value < 0.0001) with airflow velocity when averaged over daily or
313 weekly timescales (Figure 7). Here we quantify correlation using Spearman’s

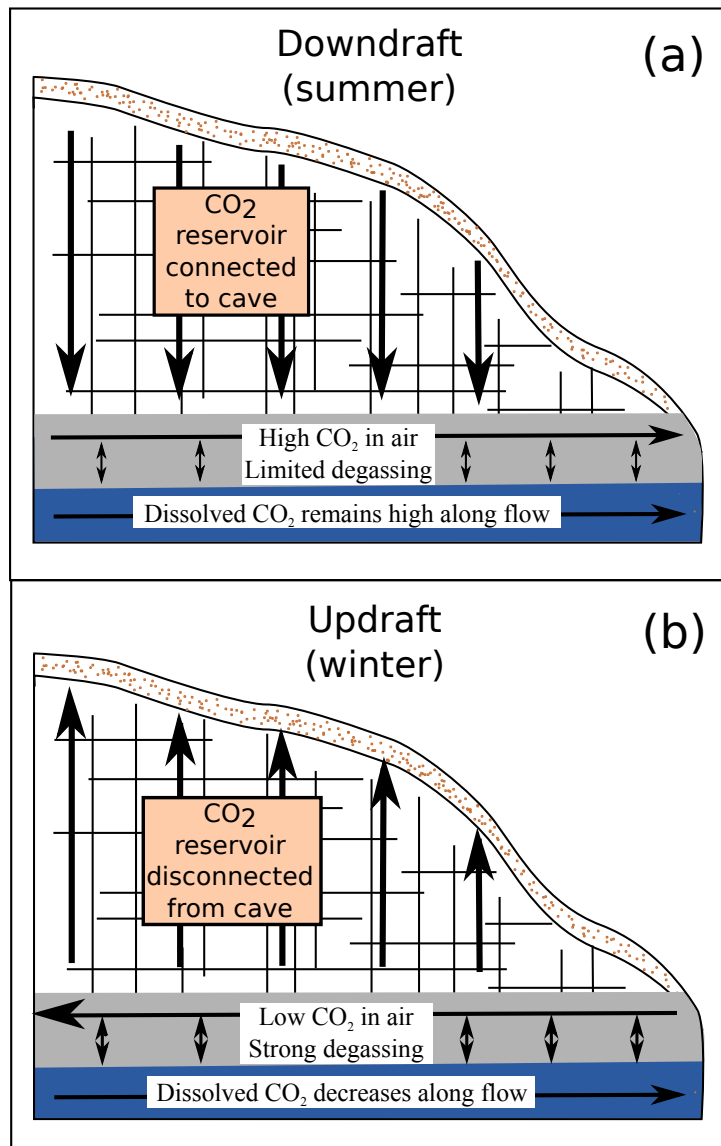


Figure 5: Conceptual model of how ventilation direction impacts dissolution rates in the cave stream: (a) During downdraft (summer conditions), air flows vertically downward through the soil and vadose zone, obtaining high CO₂. Cave air pCO₂ is high and therefore degassing of CO₂ from the cave stream is limited. Consequently, dissolved CO₂ and dissolution rates remain high along the main conduit. (b) During updraft (winter conditions), atmospheric air enters the cave through the large lower entrance and then flows upward through the high-CO₂ vadose zone. The cave air is disconnected from this high CO₂ zone and strong degassing of CO₂ occurs along the stream, reducing pCO₂ and dissolution rates. During winter storms, vertical flow of water can transport CO₂ through the vadose zone and effectively reconnect the cave stream to the CO₂ reservoir.

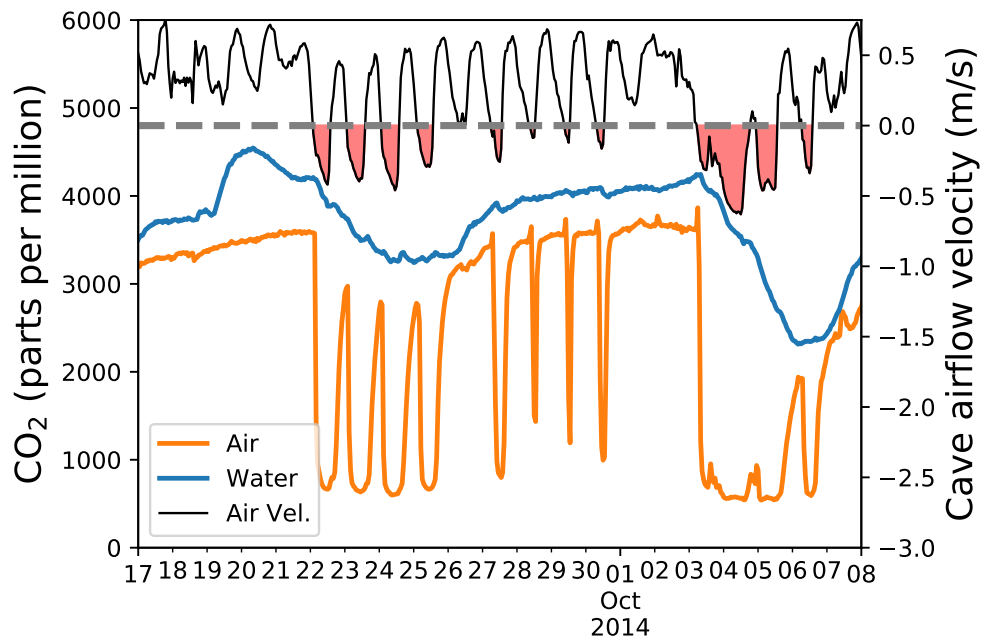


Figure 6: Time series of airflow velocity (top, black), and CO₂ concentrations in air (orange, bottom) and water (blue, middle), where the gray dashed line demarcates zero airflow velocity and the shaded red portions of the curve are periods of updraft (inward airflow). During updraft, gaseous CO₂ concentrations decrease sharply to near atmospheric concentrations. During extended periods of updraft, dissolved CO₂ also decreases. During downdraft CO₂ in the air and water increase.

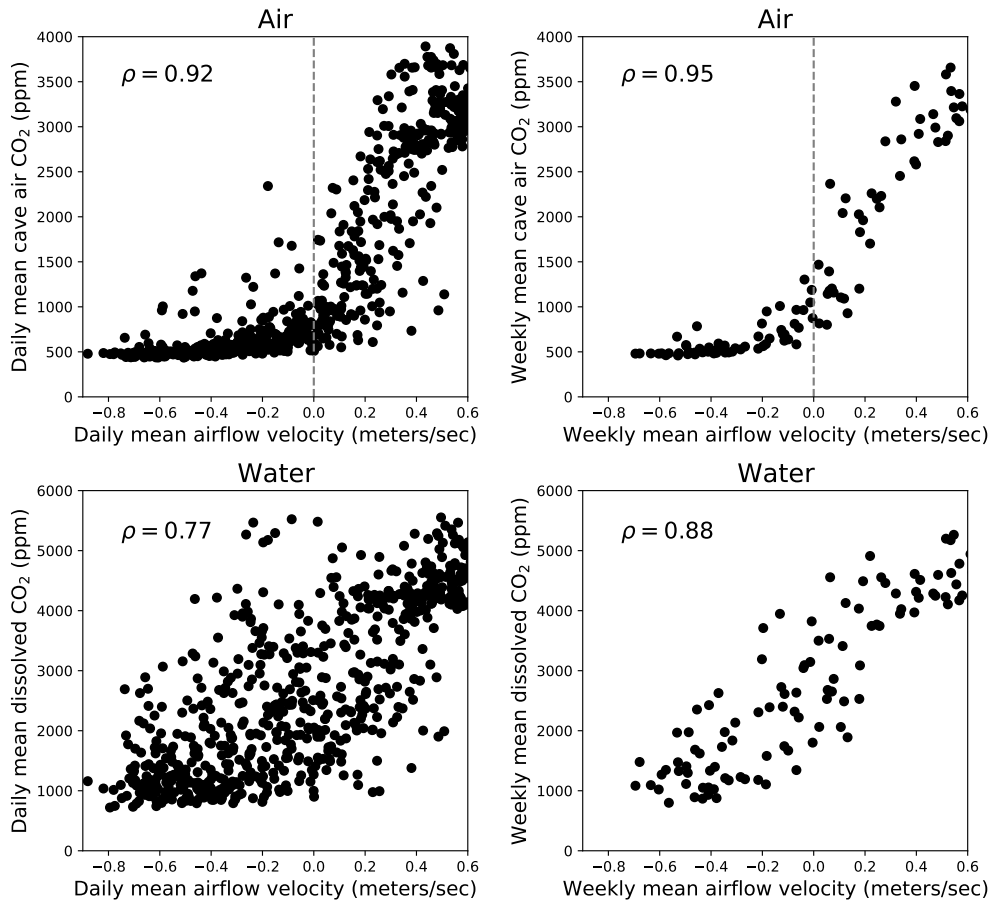


Figure 7: Relationships between airflow velocity and CO₂ concentrations in air and water averaged on daily and weekly timescales. Correlations are quantified using Spearman's rank correlation coefficient ρ . Dashed vertical lines indicate the threshold change in CO₂ concentrations that corresponds to airflow reversals (ppm = parts per million).

314 rank correlation coefficient because the relationships are non-linear (Helsel
315 and Hirsch, 2002). Correlations are stronger over the weekly timescales than
316 the daily timescales, particularly for dissolved CO₂. The gaseous CO₂ con-
317 centrations display a clear threshold near zero airflow velocity (Figure 7),
318 which divides time periods with updraft and downdraft. During periods of
319 updraft, the cave air CO₂ is typically near outside atmospheric concentra-
320 tions, whereas during downdraft, concentrations substantially increase above
321 atmospheric values. The relationship between dissolved CO₂ and cave airflow
322 does not display a clear threshold at zero cave airflow but still has a clear pat-
323 tern of lower concentrations during updraft and higher concentrations during
324 downdraft (Figure 7).

325 4.4. Dissolution rate dynamics in the cave stream

326 To examine how the dissolution rates in the stream evolve over time, we
327 calculated calcite dissolution rates for the entire time series, using both the
328 PWP and Palmer equations. The dissolution rates show a strong seasonal
329 signal that is in-phase with the seasonal CO₂ variation (Figure 8). That
330 is, there are higher rates of dissolution during the summer months, when
331 pCO₂ is also high and the water is undersaturated with respect to calcite.
332 Lower rates of dissolution occur during the winter months (frequently nega-
333 tive PWP rates), when pCO₂ is low and the water is typically supersaturated.
334 The average of this seasonal signal is near calcite saturation (or zero disso-
335 lution rate), but the stream spends slightly more time in the undersaturated
336 condition, when dissolution is active. In addition to the seasonal signal, there
337 is clear variability on daily to weekly timescales.

338 To study the chemical controls on dissolution rate variation, dissolution
339 rates averaged over daily timescales are plotted versus the two primary chem-
340 ical drivers (Figure 9): dissolved CO₂ and a proxy for dissolved load (SpC).
341 To quantify the correlations between the chemical drivers and dissolution
342 rate, we calculated Spearman's rank correlation coefficients. Both chemical
343 drivers correlate with dissolution rates (p-value<0.0001), but CO₂ is more
344 strongly correlated ($\rho = 0.84$) than SpC ($\rho = -0.3$). The cloud of points in
345 the dissolution rate-CO₂ plot (Figure 9a) shows a relatively sharp edge at
346 low dissolution rate. This edge is created by baseflow conditions, where SpC
347 displays a typical value of around 220 $\mu\text{S}/\text{cm}$.

348 In addition to direct chemical drivers, dissolution rates vary as a function
349 of external physical controls that produce variations in those chemical drivers.
350 The two most important physical controls on chemical variation at the site are

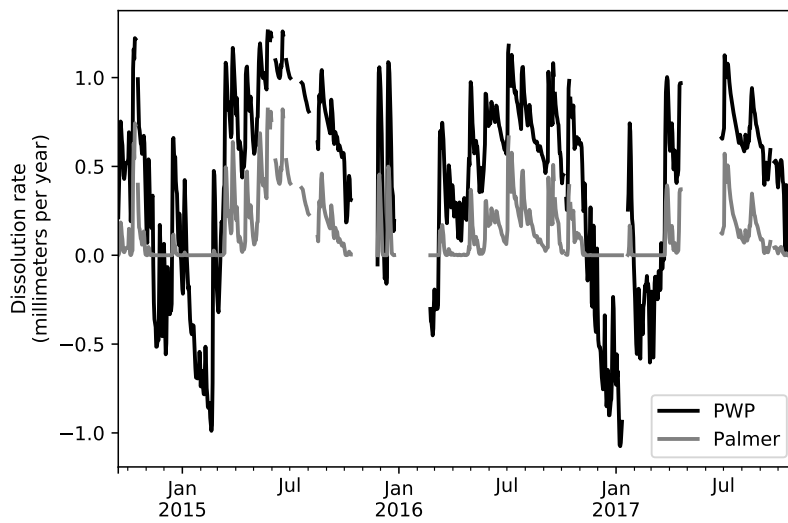


Figure 8: Calcite dissolution rates calculated from $p\text{CO}_2$ and SpC time series, where the black line depicts rates calculated using the PWP equation (which includes negative values) and the gray line indicates rates calculated using the Palmer equation. The data indicate a regular seasonal pattern in dissolution rate variability, with undersaturated conditions typical in the summer and supersaturated conditions typical in the winter.

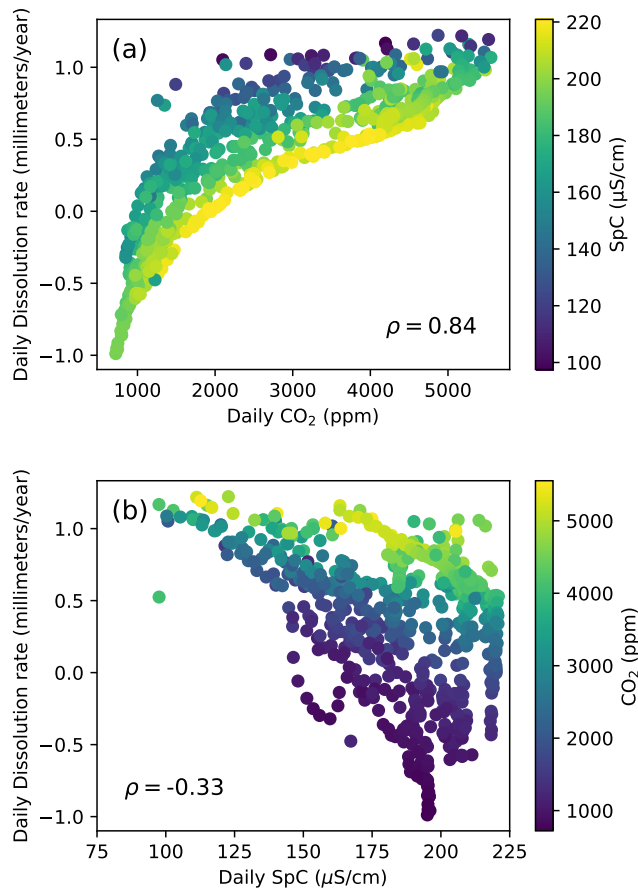


Figure 9: Relationships between daily averaged dissolution rates and (a) pCO₂ (parts per million) or (b) SpC (microsiemens per centimeter), where correlations are quantified using Spearman's rank correlation coefficient, ρ .

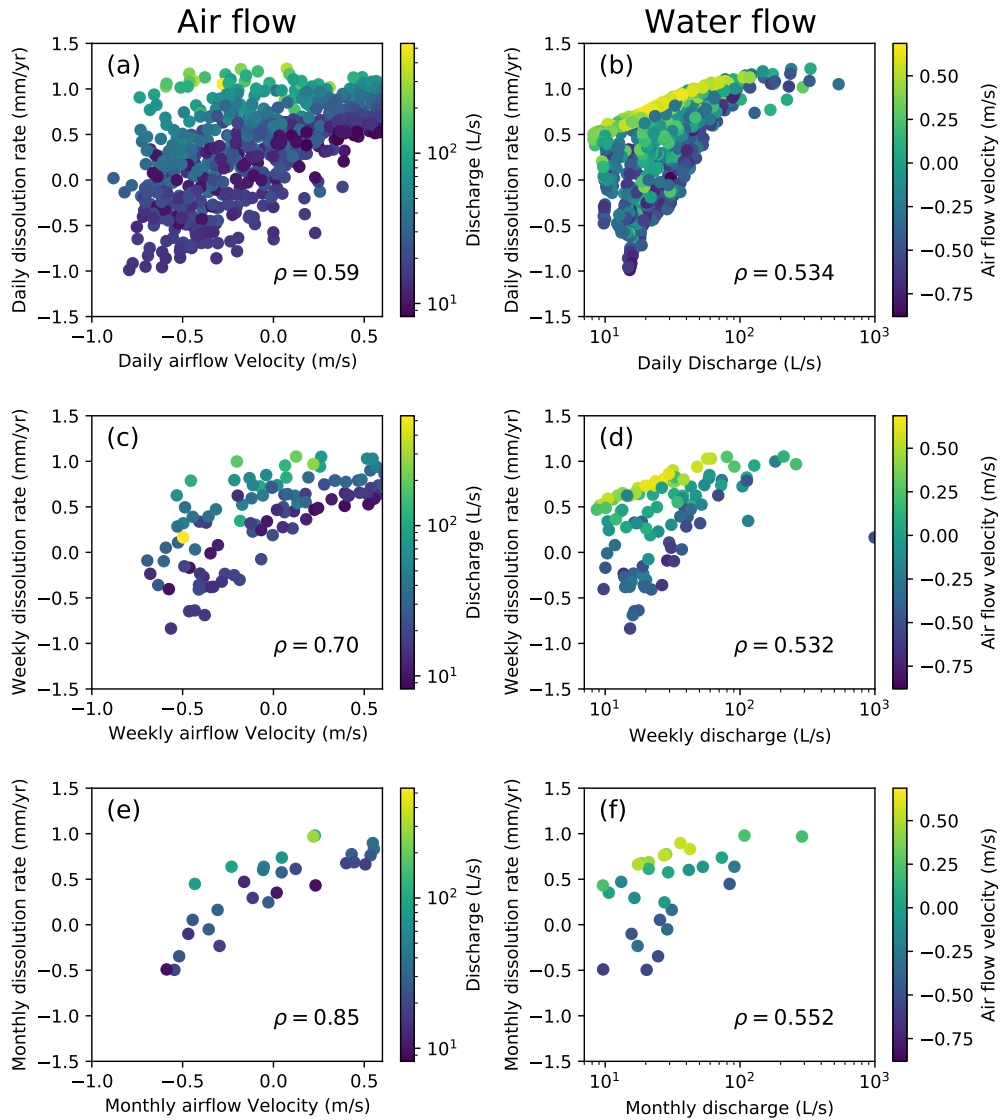


Figure 10: Relationships between dissolution rates and air flow velocity (left column: a,c,e) or stream discharge (right column: b,d,f). Each row represents rates averaged over different a time period, from daily (a,b), to weekly (c,d), to monthly (e,f). Color/shading in the left column indicates discharge and in the right column indicates air flow velocity, and correlations are quantified using Spearman's rank correlation coefficient, ρ . Units are: mm/yr = millimeters per year; m/s = meters per second; L/s = liters per second.

351 cave airflow velocity and stream discharge. Cave airflow, and particularly its
352 direction, is an important driver of dissolved CO₂, as shown above (Figures 5
353 and 7). Discharge may produce variation in both dissolved load and dissolved
354 CO₂, either through dilution during storm-event runoff or alteration of water
355 sources and flowpaths. Figure 10 shows the relationships between dissolution
356 rate and these two physical drivers over a variety of timescales from daily
357 (a,b), to weekly (c,d), to monthly (e,f). Generally, when airflow velocity is
358 positive (downdraft) and discharge is greater, dissolution rate is greater. At
359 all timescales, cave airflow displays a stronger correlation with dissolution
360 rate than discharge. The strength of the correlation between airflow velocity
361 and dissolution rate increases with the duration of the averaging. Correlation
362 with discharge is similar for all timescales and is comparable to the correlation
363 for cave airflow velocity on the daily timescale. All correlations have p-
364 values < 0.0001 except for the monthly correlation with discharge, which has
365 a p-value = 0.0018.

366 Since cave airflow velocity emerges as the strongest external driver of
367 dissolution rate variability, and because airflow direction is likely to be the
368 most important factor in determining CO₂ concentrations, we divide the
369 record into days when airflow is on average updraft (winter regime) and
370 downdraft (summer regime). Dissolution rates are higher during periods of
371 downdraft, when the cave air has higher CO₂ (Figure 11). Interestingly, there
372 is also a strong contrast in the variability of dissolution rates during the two
373 airflow regimes, with periods of updraft having much larger variability in
374 rates. This effect is further considered below as we examine how dissolution
375 rates vary during storms.

376 4.5. Dissolution rate variation during storms

377 To explore how dissolution rates vary during storms, we first examine rela-
378 tionships between dissolved CO₂ and discharge, because CO₂ is the chemical
379 parameter most strongly correlated with changes in dissolution rate (Figure
380 9). Since dissolution rates show more variability during upward airflow, one
381 hypothesis might be that airflow direction somehow modulates the variabil-
382 ity caused by changes in discharge. As an initial test of this hypothesis, we
383 examine the relationship between daily averaged values of dissolved CO₂ and
384 discharge, separated into groups of downdraft and updraft conditions (Figure
385 12). Dissolved CO₂ is correlated with discharge during periods of updraft
386 ($\rho = 0.31$, p-value < 0.0001), whereas there is no statistically significant cor-
387 relation between dissolved CO₂ and discharge during periods of downdraft

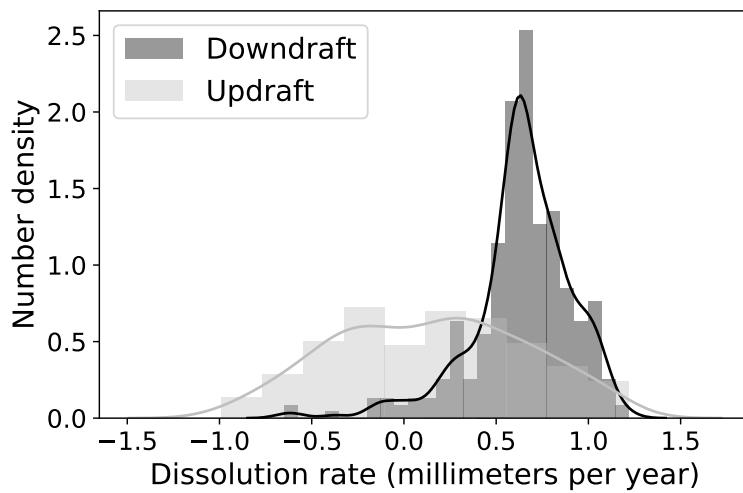


Figure 11: Distribution of dissolution rates under different airflow regimes for daily averaged dissolution rates under both downdraft (dark gray) and updraft (light gray) conditions. During downdraft dissolution rates are typically high. During updraft dissolution rates are typically lower; however they are also much more variable. Kernel density estimates are shown (solid lines) to aid visual distinction of the two overlapping distributions.

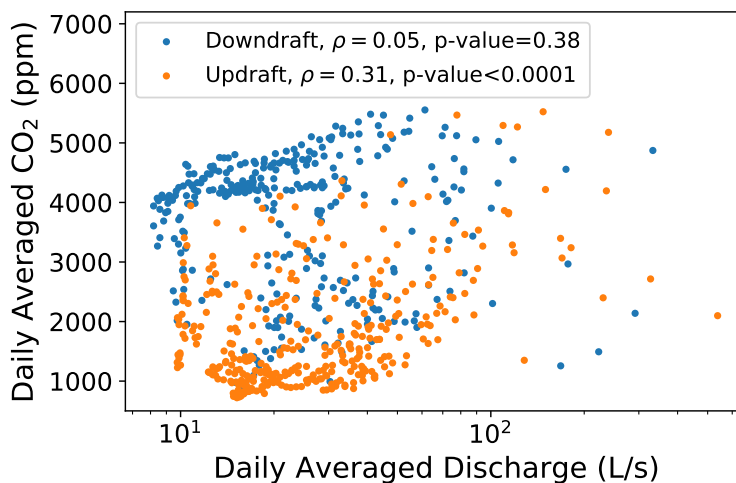


Figure 12: Relationship between discharge and CO₂ under different airflow regimes. Daily averaged values of discharge and CO₂ for periods of either downdraft (blue) or updraft (orange). Spearman's rank correlation coefficients, ρ , and respective p-values indicate that there is a moderate correlation between discharge and CO₂ during periods of updraft airflow but no statistically significant correlation during periods of downdraft airflow. Units are: ppm = parts per million; L/s = liters per second.

388 airflow ($\rho = 0.04$, p-value = 0.38).

389 To further examine the possibility that airflow modulates discharge-driven
 390 dissolution rate variation during storms, we plot time series of chemistry and
 391 estimated dissolution rates during storm events. Two typical examples are
 392 shown in Figure 13, one during downdraft (summer) conditions and one
 393 during updraft (winter) conditions.

394 The winter storm produces more variation in dissolved CO₂, which ranges
 395 from around 1000 ppm to 3500 ppm. Gaseous CO₂ remains low during most
 396 of the event because of the dominance of updraft conditions, which bring
 397 outside air quickly to the sensor location from the cave entrance. SpC varies
 398 from near maximal values, around 220 $\mu\text{S}/\text{cm}$, to 115 $\mu\text{S}/\text{cm}$. Driven by
 399 both changes in CO₂ and dissolved load, the dissolution rate changes sharply
 400 during the storm, from supersaturated conditions (-0.25 mm/yr) before the
 401 storm to highly undersaturated conditions (1.2 mm/yr) near the peak of the
 402 event. During the winter storm, estimated discharge ranged from 30 L/s to
 403 330 L/s.

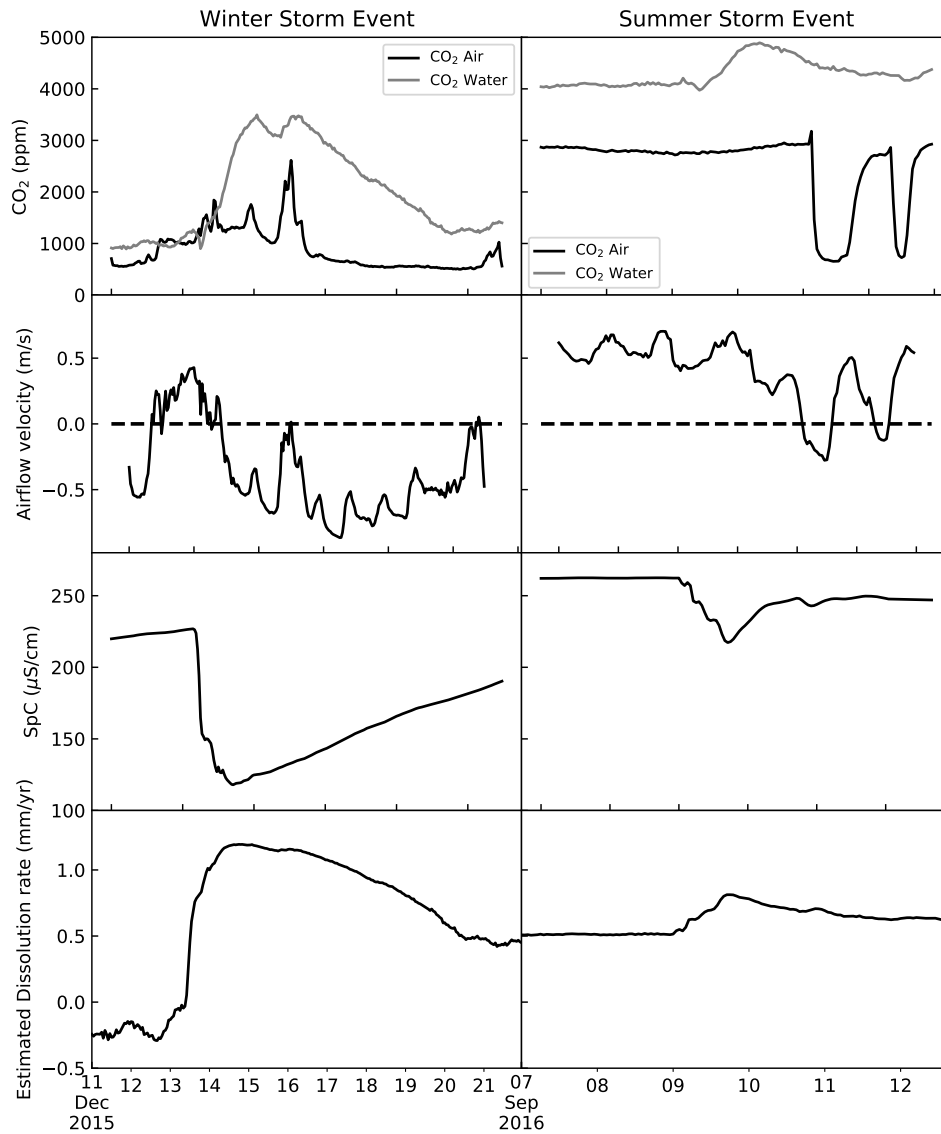


Figure 13: Variability of CO₂, airflow velocity, specific conductance (SpC), and estimated calcite dissolution rate during two example summer and winter storm events. The winter event, when airflow is primarily updraft (negative) exhibits more variation than the summer event in both dissolved CO₂ and SpC, and consequently in dissolution rate. The summer event exhibits low chemical variability. Units are: ppm = parts per million; m/s = meters per second; $\mu\text{S}/\text{cm}$ = microsiemens per centimeter; mm/yr = millimeters per year.

404 During the summer storm, downdraft conditions prevail, and, conse-
405 quently, CO₂ concentrations in the air remain relatively high around 3000 ppm,
406 except for during two brief periods of airflow reversal that follow the storm.
407 Dissolved CO₂ is already high (4000 ppm) before the start of the event and
408 peaks around 5000 ppm during the event. Therefore, there is much less vari-
409 ability of dissolved CO₂ during the summer storm than during the winter
410 storm. SpC decreases during the storm from around 255 $\mu\text{S}/\text{cm}$ to around
411 220 $\mu\text{S}/\text{cm}$, displaying less variability than during the winter storm. Disso-
412 lution rate also displays less variability, with rates around 0.5 mm/yr before
413 the storm and 0.8 mm/yr at the peak. During the summer storm, estimated
414 discharge ranged from 8.4 L/s to 80 L/s.

415 In general, winter and spring storms (periods of mostly updraft) show
416 larger changes in discharge (Figure 2), as might be expected from lower rates
417 of evapotranspiration during these cooler periods. Therefore, one possibility
418 is that the correlation between airflow direction and dissolution rate variabil-
419 ity (Figure 11) is spurious and is actually driven by differences in discharge
420 dynamics during these seasons. Because discharge has a strong negative
421 correlation to dissolved load (Figure 3), storms with greater discharge varia-
422 tion should also have greater variation in dissolved Ca, and this could drive
423 greater variation in dissolution rate.

424 To explore this possibility we identify all storm events and calculate the
425 range of dissolution rate, the average airflow velocity, and the range of dis-
426 charge during each storm over the period of record. The beginnings of storms
427 were defined as increases in discharge of at least a factor of two within a period
428 of less than two days. The end of a storm event was defined to be a return to
429 130% of the pre-storm discharge or one week after the increase in discharge,
430 whichever was shorter. Because most of the chemical variation occurs during
431 the rising limb, the dissolution rate ranges are not particularly sensitive to
432 the criteria for the end of a storm event. However, including these crite-
433 ria enables treatment of multi-peak events as a single storm. We find that
434 change in dissolution rate within a storm was much more strongly correlated
435 to mean cave air velocity during the storm ($\rho = 0.85$, p-value=0.0002) than it
436 was to the magnitude of the change in discharge ($\rho = -0.04$, p-value=0.88),
437 as is shown in Figure 14 for the storm events for which complete chemical
438 records exist. This suggests that cave airflow direction is an important con-
439 trol on dissolution rate variation during storms, and that storm dissolution
440 rate variability is not primarily driven by dilution.

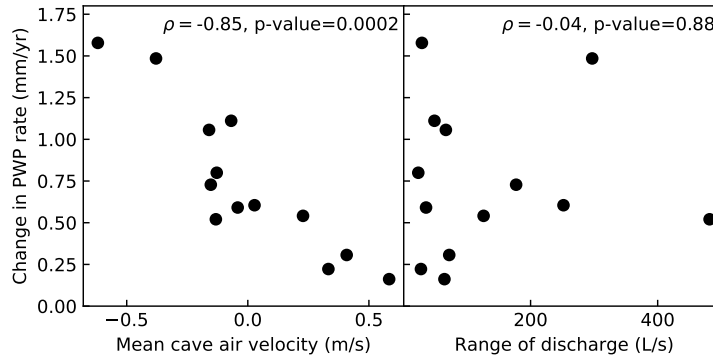


Figure 14: Correlations between storm dissolution rate range and potential controls. Average airflow velocity during a storm event is highly correlated with the range in dissolution rates during the event. The range of discharge within the event is not significantly correlated with the range in dissolution rates. Data are shown for all identified storm events during the study period for which complete chemical records were available.

441 5. Discussion

442 5.1. Controls of dissolution rate variability

443 The concept of the magnitude and frequency of erosional forces is central to understanding how temporal variations in the rates of geomorphic processes influence the long-term rates of landscape evolution and the morphology of landforms that develop (Wolman and Miller, 1960). This concept is most frequently applied in fluvial systems, where frequency relates to the recurrence interval of discharges of different magnitude. However, magnitude and frequency has also been discussed in the context of weathering processes, such as chemical solution (Goudie and Viles, 1999).

451 A variety of studies have quantified variation in rates of chemical geomorphic work at the basin scale by examining the rate of solute export as a function of river discharge (Wolman and Miller, 1960; Gunn, 1982; Schmidt, 1985). However, quantifying magnitude and frequency within the context of weathering presents some challenges, and, particularly one must be clear as to the specific process that one is attempting to quantify (Goudie and Viles, 1999). Calculating chemical weathering rates using river solutes provides a quantification of the magnitude and frequency attributes of solute export from a basin. However, since solutes are stored within the basin for some unknown time, these rates are removed from the rates of actual detachment

461 of the ions from mineral surfaces. For example, Covington et al. (2015) show
462 that in-stream calcite dissolution rates may be orders of magnitude higher
463 than basin-wide denudation rates derived from basin solute export. One
464 can imagine, similarly, that the time variability of rates of dissolution on
465 karst landscape surfaces might be quite different than the time variability in
466 basin-wide solute export rates.

467 Relatively few studies have attempted to quantify the time-variation of
468 calcite dissolution rates within karst streams or caves, or to understand the
469 controls of this variability (Groves and Meiman, 2005; Palmer, 2007b; Cov-
470 ington et al., 2015; Covington and Vaughn, 2019). The central goal of this
471 study was to examine variability in dissolution rates within a specific cave
472 stream and to develop a mechanistic understanding of the controls on that
473 variability.

474 As in previous studies (Groves and Meiman, 2005; Covington et al., 2015;
475 Covington and Vaughn, 2019), we find that the strongest chemical driver of
476 variation in dissolution rates is variation in dissolved CO_2 , which shows much
477 stronger correlation with dissolution rate at our site than does dissolved load
478 (Figure 9). In turn, dissolved CO_2 displays a strong seasonal pattern, ranging
479 from around 1000 ppm in the winter to around 5000 ppm in the summer.
480 This seasonal pattern is strongly correlated with seasonal changes in the cave
481 air CO_2 that are driven by the direction of cave airflow (Figures 2a-b and 7),
482 which is ultimately controlled by the temperature difference between cave air
483 and outside air (Equation 5). A conceptual sketch of the interactions between
484 these processes is shown in Figure 5. Review of time series over shorter
485 timescales (days to weeks) provides even stronger evidence for a mechanistic
486 connection between cave airflow and dissolved CO_2 , where switches in airflow
487 direction strongly perturb CO_2 concentrations in the cave atmosphere, and
488 the dissolved CO_2 in the cave stream responds in a lagged and muted fashion,
489 decreasing during periods of low cave air CO_2 and increasing during periods
490 of high cave air CO_2 (Figure 6).

491 Review of the entire dataset shows that, perhaps surprisingly, dissolution
492 rate is more strongly correlated with cave airflow velocity than with discharge
493 (Figure 10). The difference in the correlation strength increases moving from
494 daily to monthly timescales, suggesting that cave airflow is most important
495 in impacting the seasonal pattern though still has a strong impact on the
496 timescales of storms. Similar observations have been made on the impact of
497 cave ventilation on the saturation state of drip water and resulting seasonal
498 biases within speleothem records (Spötl et al., 2005; Banner et al., 2007;

499 Wong et al., 2011), and ventilation has also previously been argued to impact
500 spatial or temporal changes in cave stream dissolved CO₂ or dissolved load
501 (Troester and White, 1984; Jeannin et al., 2017). Gulley et al. (2014) also
502 found that seasonal cave ventilation patterns can explain seasonal changes
503 to dissolved load and dissolved CO₂ within a water table cave in Florida.
504 Therefore, the patterns observed here cohere with previous studies, though
505 our data provide much higher time resolution to examine the connections
506 between ventilation and cave stream saturation state in more detail.

507 Though the time series suggest that cave airflow direction is an important
508 control of the seasonal oscillation of dissolved CO₂, there may be additional
509 drivers. Specifically, CO₂ production in the soil through microbial decay and
510 root respiration is known to vary with surface temperature and solar radiation
511 (Hibbard et al., 2005; Lloyd and Taylor, 1994). At a nearby site with a similar
512 hydrogeological setting, Covington and Vaughn (2019) observed a strong
513 seasonal signal (range \approx 20,000 ppm) in dissolved CO₂ at Langle Spring,
514 Arkansas, which is thought to drain an unventilated portion of the karst
515 aquifer. They hypothesized that this signal derived from seasonal changes in
516 subsurface CO₂ production. It is uncertain how much of the seasonal signal
517 in dissolved CO₂ at Blowing Springs might also be a function of changes in
518 the rate of CO₂ production.

519 In contrast to the seasonal respiration-driven pattern, some karst aquifers
520 that exhibit higher pCO₂ at depth than in the soil have very little seasonal
521 CO₂ variation at depth (Atkinson, 1977a). A prior study at Blowing Springs
522 Cave measured soil CO₂ concentrations, with summer values frequently be-
523 ing above what we observe in the cave stream and winter values frequently
524 being below (Knierim et al., 2017). Additionally, the study used stable car-
525 bon isotopes to quantify the mixture of atmospheric CO₂ versus unsaturated
526 zone CO₂ (produced via respiration/decomposition) in the cave atmosphere.
527 Knierim et al. (2017) found that the proportion varied seasonally and, addi-
528 tionally, that there were different mixing lines for each season, highlighting
529 seasonally variable unsaturated zone CO₂ sources. At the least, these ob-
530 servations suggest that there is some storage of CO₂ in the vadose zone
531 that might reduce seasonal variation in the cave. The few available spot
532 measurements of dissolved CO₂ at the upstream sump in Blowing Springs
533 Cave indicate a range of approximately 1500 ppm between summer and win-
534 ter measurements (Young, 2018), in contrast to the range of approximately
535 5000 ppm that we observe near the downstream end of the cave. However,
536 it is also unclear how much ventilation might occur within the portion of the

537 aquifer that is upstream of the sump. Therefore, whereas there is a clear
538 impact of cave ventilation on the annual CO₂ cycle, there may also be a sea-
539 sonal signal driven by production. The magnitude of that production signal
540 is uncertain.

541 The mechanistic link between cave airflow direction and dissolved CO₂
542 in the stream is generated because the primary CO₂ source for the cave air
543 can either be upwind or downwind of the main cave stream (Figure 5). The
544 primary source of CO₂ to the cave atmosphere is a CO₂ reservoir within the
545 soil and vadose zone above the cave. During periods of downdraft (summer
546 regime) ventilation brings gases from this reservoir into the cave, maintain-
547 ing a high pCO₂ within the cave air that limits degassing of CO₂ from the
548 cave stream (Figure 5a). During periods of updraft (winter regime) venti-
549 lation brings fresh outside air into the cave, reducing the pCO₂ of the cave
550 air and enhancing degassing of CO₂ from the stream (Figure 5b). Though
551 the cave has strong ventilation during both summer and winter conditions,
552 the restricted nature of the airflow pathways through the vadose zone must
553 produce a sufficiently high surface area to volume ratio that air transiting
554 this zone obtains a high pCO₂.

555 *5.2. Dissolution rate variability during storms and the role of airflow*

556 Whereas storms play a secondary role in driving variability in dissolu-
557 tion rates, there are still statistically significant correlations ($\alpha=0.05$)
558 between discharge and dissolution rate (Figure 10b). We can observe these
559 variations clearly on the basis of individual storms, and see that they are
560 driven by a combination of dilution and increasing dissolved CO₂ (Figure
561 13). Interestingly, airflow direction also appears to modulate the dissolution
562 rate variability within storms, with greater storm variability during updraft
563 conditions. This is supported by at least three observations:

- 564 1. Variation in dissolution rates is much greater during updraft than
565 downdraft (Figure 11);
- 566 2. Dissolved CO₂ is positively correlated with discharge during updraft
567 but not during downdraft (Figure 12);
- 568 3. Dissolution rate range during individual storms is correlated to the
569 airflow velocity but not to the range of discharge during the storm
570 (Figure 14).

571 It is perhaps counterintuitive that cave airflow direction should have any
572 importance for dissolution rate variation during storms. However, the ob-

573 served pattern can be explained using an existing conceptual model for va-
574 dose zone CO₂ within karst (Mattey et al., 2016) and a basic mathematical
575 framework for transport of CO₂ within the karst vadose zone (Covington,
576 2016). Mattey et al. (2016) argue, based on eight years of field measure-
577 ments at the Rock of Gibraltar and other observations of deep CO₂ within
578 karst systems (Atkinson, 1977a; Wood, 1985; Wood and Petraitis, 1984), that
579 karst vadose zones contain a body of “ground air,” which is a reservoir of
580 CO₂ produced by the microbial decay of organic matter that has infiltrated
581 to depth. Cave air is considered to be a mixture of surface air with ground
582 air, where the percentages depend largely on the outside temperature and
583 the resulting direction of air circulation through the vadose zone.

584 Other work has suggested that the CO₂ in cave air is often associated
585 with root respiration of the deepest rooting plants (Breecker et al., 2012),
586 again suggesting production at depth. At Blowing Springs Cave, the carbon
587 isotope ratios of CO₂ are consistent with soil/root respiration (Knierim et al.,
588 2017), so it is unclear whether the source of deep vadose zone CO₂ might be
589 particulate organic matter or from root respiration. However, to explain the
590 observations, we hypothesize that there is a substantial volume of CO₂ stored
591 at depth in the vadose zone.

592 During winter (periods of cave updraft), storms bring water that is charged
593 with CO₂, frequently 2000–4000 ppm. These concentrations are substantially
594 higher than typically observed in soil at the site during fall/winter (1500 ppm)
595 in a prior study (Knierim et al., 2017). This observation supports the con-
596 ception of a reservoir of high pCO₂ within the vadose zone (Atkinson, 1977a;
597 Mattey et al., 2016). Additionally, a simple model of CO₂ transport within a
598 vertical fracture suggests that vertical flow of water through karst fractures
599 can efficiently redistribute CO₂ within the subsurface, pushing it to greater
600 depth (Covington, 2016). Observations of hysteresis between discharge and
601 dissolved CO₂, with higher CO₂ during the recession, have also been inter-
602 preted as indicating that later arriving diffuse recharge water can transport
603 soil and vadose zone CO₂ into karst conduits. Therefore, it is physically
604 plausible that vertical flow of water through the vadose zone during a storm
605 could effectively transport a pulse of CO₂ to the water table.

606 During winter storms, we hypothesize that storm water obtains CO₂ from
607 a reservoir of ground air and transports it quickly to the cave stream, produc-
608 ing the CO₂ pulses that drive higher rates of variation in dissolution during
609 winter events. This produces variation in part because the winter airflow
610 regime has disconnected the cave stream from the CO₂ source (Figure 5b),

611 reduced the $p\text{CO}_2$ of the cave stream, and the pulse of high CO_2 has a large
612 effect. On the contrary, in the summer (downdraft) airflow regime the cave
613 air is already in contact with the ground air (Figure 5b), as the air is entering
614 the cave via the soil and vadose zone. Therefore, degassing is reduced and
615 the cave stream is maintained at high $p\text{CO}_2$. Consequently, summer storms
616 produce much less variation in CO_2 within the cave stream and therefore less
617 variation in dissolution rate. This conceptual model is also supported by pre-
618 vious work at Blowing Springs Cave where isotopic disequilibrium between
619 dissolved inorganic carbon (DIC) in the cave stream and CO_2 in the cave
620 air was greater during winter periods, when the cave stream is disconnected
621 from the CO_2 source, but approached equilibrium during summer, when cave
622 air CO_2 was higher (Knierim et al., 2017).

623 *5.3. Dissolution rate variation in the context of similar studies*

624 Since discharge is not the primary driver of variation in dissolution rates
625 at the study site, normal concepts of magnitude and frequency break down, as
626 they are based on flood recurrence intervals. To estimate rates of geomorphic
627 work in the cave stream, we are better off asking, “Which way is it blowing?”
628 rather than, “How much is it flowing?” However, this pattern is seemingly
629 not a universal one, and it is worth putting into the context of the limited
630 set of other studies of dissolution rate variation in karst conduits.

631 First we compare against the nearby study of Langle and Copperhead
632 Springs (Covington and Vaughn, 2019), two karst springs located in the
633 same limestone layer and climate setting as Blowing Springs Cave. These
634 two springs compose a karst underflow-overflow system, where Langle Spring
635 is completely phreatic and carries most of the flow at low discharge. Lan-
636 gle and Copperhead Spring both exhibit strong seasonal CO_2 variation that
637 is the strongest control on dissolution rate. Here again, variation driven
638 by discharge is secondary. Data suggest that Langle drains a relatively
639 small phreatic conduit, which has no ability to ventilate. Langle Spring
640 has the highest variation in CO_2 concentration of any of the available studies
641 of dissolution rates within karst conduits, with summer values that exceed
642 20,000 ppm and winter values around 3,000 ppm. One potential reason for
643 the higher CO_2 concentrations and strong production-related signal is that
644 landuse in the spring recharge zone is predominantly pasture, and grasslands
645 have higher CO_2 production rates than forested areas (Smith and Johnson,
646 2004; Knierim et al., 2015a, 2017). Copperhead Spring has peak values in

647 early summer around 15,000 ppm and then late summer values around 5000–
648 6000 ppm, which are similar to peak summer values at Blowing Spring. The
649 sudden decrease in CO₂ at Copperhead Spring in the early summer coin-
650 cides with a discharge threshold. Below this threshold, the data suggest that
651 the cave system feeding this spring begins to ventilate, and CO₂ decreases
652 dramatically as a result of the onset of ventilation (Covington and Vaughn,
653 2019). Therefore, if we want to estimate dissolution rates at Langle Spring,
654 we need to consider variability in CO₂ sources related to soil CO₂ production,
655 and might ask ourselves, “Is it growing?”. Whereas, at Copperhead Spring,
656 which is intermittently ventilated, we could ask, “Is it blowing?”

657 In the two other cave streams where dissolution rate or saturation state
658 has been quantified as a function of discharge (Groves and Meiman, 2005)
659 or recurrence interval (Palmer, 2007b), the cave water was supersaturated
660 during most of the study period, with only short periods of active dissolution
661 occurring at high flow. Groves and Meiman (2005) study the Logsdon River
662 in Mammoth Cave, Kentucky, and Palmer (2007b) studies McFail’s Cave,
663 New York. Both studies found that the majority of the dissolution occurs in
664 the top 5% flow regime. Therefore, these sites fall more into the standard
665 magnitude and frequency framework, where active dissolution is driven by
666 high flow events.

667 One reason for the tendency toward supersaturation at these two sites
668 may be that they are more highly ventilated than any of the other study
669 sites. Mammoth Cave is the longest cave in the world (Gunn, 2004), has
670 many entrances, and is, consequently, well-ventilated. This high density of
671 entrances may produce relatively low CO₂ concentrations in the cave air
672 during all seasons. Therefore, water flows through the soil and vadose zone
673 dissolving calcite under relatively high pCO₂ conditions, then it enters the
674 cave stream, is brought to much lower pCO₂, and becomes supersaturated.
675 Storm events may in part increase dissolution rates by reducing ventilation
676 when portions of the system flood shut. During the largest flood event in the
677 study, Logsdon River remained under pipefull flow conditions for 114 hours
678 (Groves and Meiman, 2005). An additional factor that may create variability
679 with discharge is the nature of recharge to the system. Approximately 40% of
680 the recharge to Logsdon River is allogenic (from streams flowing off of sand-
681 stone caprock). It is plausible that flow from non-carbonates, and changes
682 to the percentage of that flow during floods, could increase the sensitivity of
683 dissolution rates to discharge (Atkinson, 1977b; Scanlon and Thrailkill, 1987;
684 Worthington et al., 1992). Palmer (2007b) also describes McFail’s Cave as

685 “well-aerated,” and suggests that the cave stream is supersaturated because
686 of ventilation and degassing of CO₂. Therefore, it is plausible that episodic
687 storm-driven dissolution is a common pattern within highly ventilated karst
688 conduit systems, which typically have low concentrations of dissolved CO₂.

689 5.4. *The role of ventilation over the history of cave evolution*

690 Taken within the context of prior studies (Groves and Meiman, 2005;
691 Palmer, 2007b; Covington and Vaughn, 2019), the data presented here elu-
692 cidate how ventilation may drive changes in dissolution rates within karst
693 conduits as they evolve. The observed behaviors can be arranged on an
694 axis of increasing ventilation (Figure 15). Except during periods of baselevel
695 aggradation, karst systems will also tend to evolve along this axis over time,
696 from no ventilation at the beginning toward highly ventilated as they mature.

697 During the first stage of karst conduit evolution, the pre-breakthrough
698 stage (Figure 15a), the penetration length of undersaturated water is less
699 than the length of the incipient conduit (Dreybrodt, 1996; Covington et al.,
700 2012). Consequently, the closed-system conditions within the flowpath lead
701 to the consumption of CO₂ that is not replenished. This resulting reduction
702 of CO₂ along the flowpath greatly reduces dissolution rates at depth.

703 Once breakthrough occurs, and the penetration length exceeds the flow-
704 path length, then water can traverse the conduit without substantially re-
705 duced pCO₂ despite the closed-system conditions (Covington and Vaughn,
706 2019). This is the stage that we observe at Langle Spring (Figure 15b), the
707 pattern that we refer to as, “Is is growing?” This stage shows the highest
708 average dissolution rates among the study sites compared here. These high
709 rates are maintained because the water is at high pCO₂ and has no means
710 of degassing that CO₂. At Langle Spring, there is a strong seasonal signal
711 driven by CO₂ production. However, some karst springs have very low an-
712 nual variation in pCO₂ (Atkinson, 1977a), so this seasonal pattern is not
713 universal. Why some karst systems have a strong production-related signal,
714 and some do not, remains an open question.

715 The third stage, “Is is blowing?” represents the onset of intermittent
716 ventilation (Figure 15c), where sometimes the karst system is ventilated and
717 sometimes it is not. In the case of Copperhead Spring, this switch is driven
718 by changes in water level. The temporal changes in dissolution rate at this
719 site show a seasonal signal, but superimposed on that seasonal signal is a
720 strong switching behavior where periods of ventilation dramatically reduce
721 the dissolution rates.

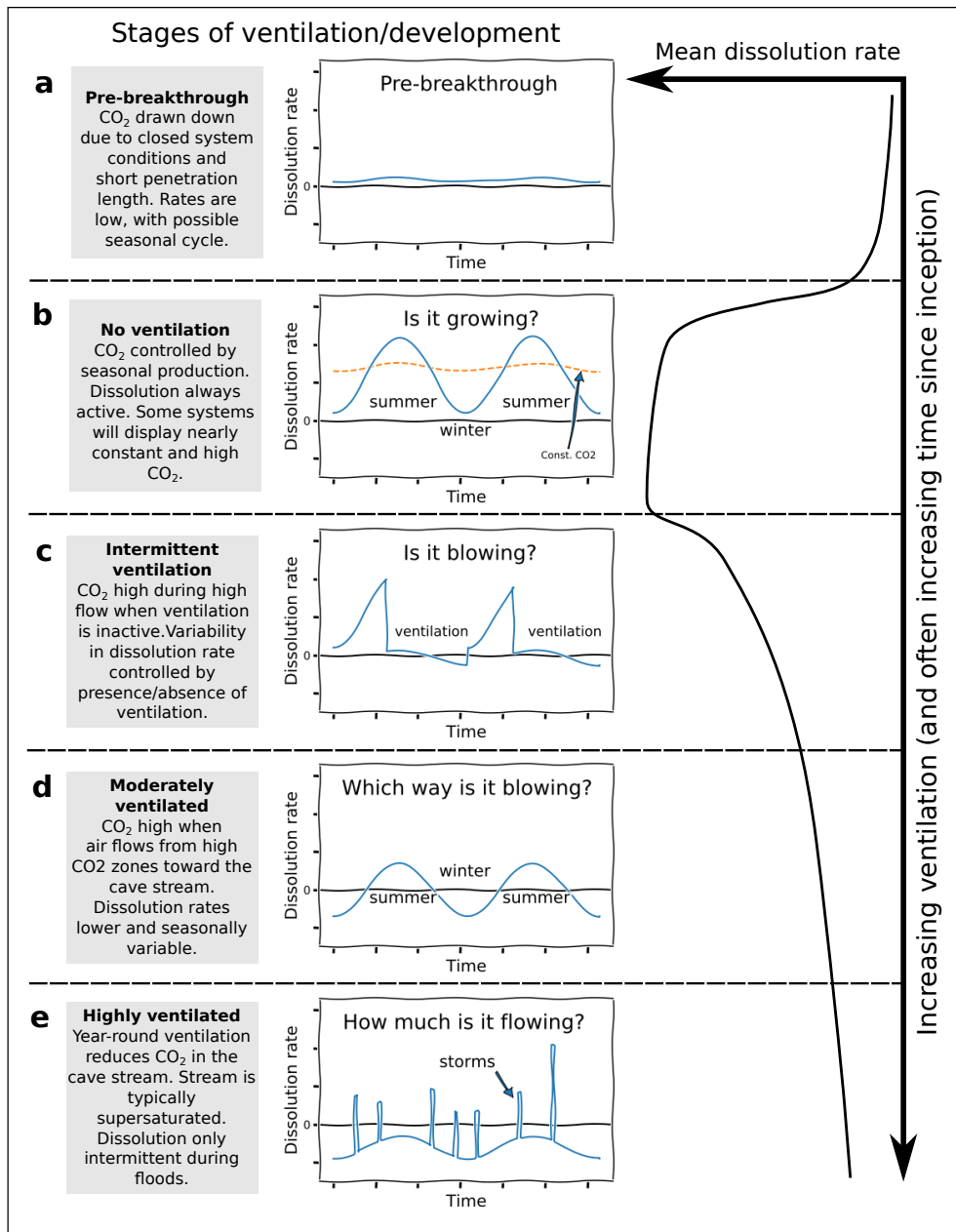


Figure 15: Patterns of observed dissolution rate variation from this and other studies and how they relate to ventilation strength and resulting CO₂ dynamics. Except during periods of baselevel aggradation, caves will typically evolve toward being more ventilated over time.

722 The fourth stage, moderately ventilated, is observed at Blowing Springs
723 Cave (Figure 15d). During this stage the conduit undergoes continuous ven-
724 tilation. However, the direction of airflow strongly impacts dissolution rates.
725 We ask, “Which way is it blowing?” The seasonal ventilation patterns that
726 are driven by chimney effect airflow create a seasonal pattern in dissolution
727 rate as the CO₂ source switches between being upwind and downwind of the
728 cave stream. The seasonal pattern is more muted than in the previous two
729 stages, and the average dissolution rates are lower. During winter periods
730 the stream is mostly supersaturated. During summer periods it is aggressive.

731 At Blowing Springs, we see secondary variability driven by storms, which
732 typically increase dissolution rates. However, even this storm variation is
733 modulated by airflow direction. To create the moderately ventilated pattern
734 of dissolution rate variability, the CO₂ of air passing through the zone of CO₂
735 sources must be strongly influenced by those sources. The exact physical
736 requirements for this influence are unclear. However, the rate and spatial
737 distributions of CO₂ production may be important. Furthermore, the air
738 pathways must have a sufficiently high surface area to volume ratio in order
739 to create effective exchange of CO₂. This may be more likely if airflow is
740 divided between many smaller pathways. Clearly, if an air pathway is too
741 open, then it will rapidly bring in outside air that reduces the pCO₂.

742 The final stage is a highly ventilated cave (Figure 15e) and is illustrated
743 by prior studies at Mammoth Cave and McFail’s Cave. Here, we return to
744 the more standard framework for considering variation in geomorphic work
745 within a stream, “How much is it flowing?” Within these systems, venti-
746 lation is sufficiently strong that the stream is normally in supersaturated
747 conditions. There may still be a seasonal variation in CO₂ (Groves and
748 Meiman, 2005), but dissolution primarily occurs during short-term high-flow
749 events. This variation may be driven by dilution, particularly in the case of
750 allogenic recharge, and may also be driven by temporary shutoff or reduction
751 of ventilation as many conduits transition into full pipe conditions during a
752 flood. Pulses of CO₂ brought through the vadose zone by water may also
753 impact cave stream CO₂, as observed at Blowing Springs Cave.

754 After initial conduit breakthrough (2nd stage, Figure 15), the overall pat-
755 tern is one of increasing ventilation and, as a result, decreasing pCO₂ and
756 decreasing dissolution rates (Palmer, 2007b). Therefore, we might expect
757 that chemical erosion rates within cave streams gradually reduce over the
758 history of evolution, except perhaps during periods of base level rise, where
759 more conduits would become flooded. This trend toward reduced chemical

760 erosion rates over time also has implications for the importance of mechan-
761 ical erosion within cave streams. Since instantaneous chemical erosion rates
762 are limited to relatively low magnitudes in comparison to mechanical erosion
763 (Covington et al., 2015), this result suggests that mechanical erosion pro-
764 cesses should become much more important once caves are well-ventilated.
765 For the well-ventilated end member, only intermittent dissolution is observed
766 during floods. These same flood events are likely to overcome thresholds for
767 transport of sediment and consequent mechanical erosion. Using the tortoise
768 and the hare analogy (Simms, 2004), chemical erosion processes are most
769 effective when they occur nearly continuously (tortoise). If chemical erosion
770 processes become intermittent, mechanical erosion is likely to dominate.

771 While we have sketched a broad hypothesis about the importance of ven-
772 tilation in controlling the rate of calcite dissolution within karst conduits,
773 and how that role might evolve as a karst system matures, the observed pat-
774 terns come from a relatively limited set of karst systems that are far from
775 spanning the full range of climatic and geological settings within which karst
776 is found. Therefore, there are likely other potential controls on dissolution
777 rate variability and perhaps other ways in which ventilation interacts with
778 CO₂ dynamics. The conceptualization in Figure 15 is relatively simplistic,
779 and it seems likely to grow in complexity as further sites are studied and
780 more dimensions of the problem are understood. Importantly, all of the
781 sites discussed are dominated by autogenic recharge. It seems plausible that
782 sites dominated by allogenic recharge will display somewhat different dynam-
783 ics. For example, ventilation may not bring water to a supersaturated state,
784 because dissolved load is always sufficiently low. Dilution may be more im-
785 portant. However, patterns of CO₂ production and degassing have also been
786 shown to control spatial patterns of dissolution within allogenicly recharged
787 systems (Covington et al., 2013).

788 Here we have categorized each study site into a single pattern/stage of
789 Figure 15, but most karst systems will contain a range of ventilation con-
790 ditions within them. Therefore, the presented stages may also represent
791 spatial contrasts in dissolution rate dynamics within different portions of a
792 karst system that have different ventilation strengths. Processes such as CO₂
793 production, ventilation, and gas exchange are currently absent from numeri-
794 cal models of speleogenesis. Developing and exploring mathematical models
795 for these processes would aid future understanding of the long-term inter-
796 actions among ventilation, CO₂ dynamics, and calcite dissolution and how
797 they influence the rates and patterns of cave development.

798 **6. Conclusions**

799 We collected time series data from a stream cave in Arkansas to study the
800 temporal variation in calcite dissolution rates and the factors that drive them.
801 Ventilation of the cave atmosphere is driven by external temperature changes
802 through the process of chimney effect airflow. The direction of air flow is
803 the primary control on gaseous CO₂ within the cave atmosphere, with low
804 CO₂ during periods with updraft, when the cave is effectively ventilated by
805 outside air, and high CO₂ during periods of downdraft, when outside air flows
806 through a zone of high CO₂ before entering the main cave passage. In turn,
807 dissolved CO₂ in the cave stream is strongly impacted by the concentration of
808 CO₂ in the cave atmosphere, generating a seasonal variation in dissolved CO₂
809 that emerges as the primary driver of dissolution rate variability within the
810 cave stream. Dissolution rate is more strongly correlated with cave airflow
811 direction than it is with discharge, indicating that the standard framework
812 of geomorphic work partitioned by flood stage is inappropriate for this site.
813 We also find that the variations of dissolution rates during individual storm
814 events are modulated by airflow direction, with more variation occurring
815 during updraft (winter) conditions. We compare the results from this study
816 with prior studies of dissolution rate variability within karst systems and
817 propose a preliminary framework to explain the different observed patterns
818 of dissolution rate variation along an axis of increasing cave ventilation. We
819 suggest that the onset of ventilation reduces the rates of chemical erosion
820 within karst systems, and that as karst systems mature they will generally
821 evolve toward greater ventilation and lower dissolution rates. This effect may
822 accentuate the importance of mechanical erosion during the later stages of
823 cave evolution.

824 **Acknowledgments**

825 We thank Joshua Blackstock, Alex Breeding, Brandon Conlon, Max Cooper,
826 Katarina Kosič, Joe Myre, Matija Perne, Evan Thaler, and for assistance in
827 the field. This material is based upon work supported by the National Sci-
828 ence Foundation under Grant No. EAR 1226903. Any opinions, findings,
829 and conclusions or recommendations expressed in this material are those of
830 the authors and do not necessarily reflect the views of the NSF. Any use of
831 trade, firm, or product names is for descriptive purposes only and does not
832 imply endorsement by the U.S. Government.

833 **Data Availability**

834 The data used in this manuscript and the python code that was used to
835 analyze the data and create the figures are provided in a Github repository
836 that is archived on Zenodo: <https://doi.org/10.5281/zenodo.3839802>.

837 **References**

- 838 Adamski, J.C., Petersen, J.C., Freiwald, D.A., Davis, J.V., 1995. Environ-
839 mental and hydrologic setting of the Ozark Plateaus study unit, Arkansas,
840 Kansas, Missouri, and Oklahoma. US Geological Survey Water-Resources
841 Investigations Report 94, 69.
- 842 Atkinson, T., 1977a. Carbon dioxide in the atmosphere of the unsaturated
843 zone an important control of groundwater hardness in limestones. *Journal*
844 *of Hydrology* 35, 111–123.
- 845 Atkinson, T., 1977b. Diffuse flow and conduit flow in limestone terrain in the
846 Mendip Hills, Somerset (Great Britain). *Journal of Hydrology* 35, 93–110.
- 847 Badino, G., 2010. Underground meteorology - What's the weather under-
848 ground? Podzemna meteorologija: Kakšno je vreme v podzemlju?. *Acta*
849 *Carsologica* 39, 427–448.
- 850 Banner, J.L., Guilfoyle, A., James, E.W., Stern, L.A., Musgrove, M., 2007.
851 Seasonal Variations in Modern Speleothem Calcite Growth in Central
852 Texas, U.S.A. *Journal of Sedimentary Research* 77, 615–622.
- 853 Blackstock, J.M., Covington, M.D., Perne, M., Myre, J.M., 2019. Moni-
854 toring Atmospheric, Soil, and Dissolved CO₂ Using a Low-Cost, Arduino
855 Monitoring Platform (CO₂-LAMP): Theory, Fabrication, and Operation.
856 *Frontiers in Earth Science* 7.
- 857 Brahana, J.V., 2011. Ten Relevant Karst Hydrogeologic Insights Gained
858 from 15 Years of In Situ Field Studies at the Savoy Experimental Water-
859 shed, in: Kuniatsky, E. (Ed.), US Geological Survey Karst Interest Group
860 Proceedings: Fayetteville, Arkansas: April 26-29, 2011, US Dept. of the
861 Interior, US Geological Survey. pp. 132–141.

- 862 Breecker, D.O., Payne, A.E., Quade, J., Banner, J.L., Ball, C.E., Meyer,
863 K.W., Cowan, B.D., 2012. The sources and sinks of CO₂ in caves under
864 mixed woodland and grassland vegetation. *Geochimica et Cosmochimica*
865 *Acta* 96, 230–246.
- 866 Covington, M., Perne, M., 2015. Consider a cylindrical cave: A physicist's
867 view of cave and karst science. *Acta Carsologica* 44, 363–380.
- 868 Covington, M., Vaughn, K., 2019. Carbon dioxide and dissolution rate dy-
869 namics within a karst underflow-overflow system, Savoy Experimental Wa-
870 tershed, Arkansas, USA. *Chemical Geology* 527, 118689.
- 871 Covington, M.D., 2007. Map of Blowing Springs Cave, Bella Vista, Arkansas.
872 Boston Mountain Grotto, Fayetteville, AR.
- 873 Covington, M.D., 2016. The importance of advection for CO₂ dynamics
874 in the karst critical zone: An approach from dimensional analysis, in:
875 *Geological Society of America Special Papers: Caves and Karst Across*
876 *Time*. Geological Society of America. volume 516, pp. 113–127.
- 877 Covington, M.D., Gulley, J.D., Gabrovšek, F., 2015. Natural variations in
878 calcite dissolution rates in streams: controls, implications, and open ques-
879 tions. *Geophysical Research Letters* 42, 2836–2843.
- 880 Covington, M.D., Luhmann, A.J., Wicks, C.M., Saar, M.O., 2012. Process
881 length scales and longitudinal damping in karst conduits. *Journal of Geo-*
882 *physical Research* 117, 1–19.
- 883 Covington, M.D., Prelovšek, M., Gabrovšek, F., 2013. Influence of CO₂
884 dynamics on the longitudinal variation of incision rates in soluble bedrock
885 channels: Feedback mechanisms. *Geomorphology* 186, 85–95.
- 886 Dreybrodt, W., 1996. Principles of early development of karst conduits under
887 natural and man-made conditions revealed by mathematical analysis of
888 numerical models. *Water Resources Research* 32.
- 889 Farrant, A.R., Smart, P.L., 2011. Role of sediment in speleogenesis; sedi-
890 mentation and paragenesis. *Geomorphology* 134, 79–93.
- 891 Ford, D.C., Williams, P., 2007. *Karst Hydrogeology and Geomorphology*.
892 John Wiley and Sons, Chichester, West Sussex, England.

- 893 Goudie, A.S., Viles, H.A., 1999. The frequency and magnitude concept in
894 relation to rock weathering. *Zeitschrift für Geomorphologie Supplement*
895 *Volumes* , 175–189.
- 896 Groves, C.G., Meiman, J., 2005. Weathering, geomorphic work, and karst
897 landscape evolution in the Cave City groundwater basin, Mammoth Cave,
898 Kentucky. *Geomorphology* 67, 115–126.
- 899 Gulley, J., Martin, J., Moore, P., 2014. Vadose CO₂ gas drives dissolution
900 at water tables in eogenetic karst aquifers more than mixing dissolution.
901 *Earth Surface Processes and Landforms* 39, 1833–1846.
- 902 Gunn, J., 1982. Magnitude and frequency properties of dissolved solids trans-
903 port. *Zeitschrift für Geomorphologie* 26, 505–511.
- 904 Gunn, J., 2004. *Encyclopedia of caves and karst science*. Taylor & Francis,
905 New York, NY.
- 906 Helsel, D.R., Hirsch, R.M., 2002. *Statistical methods in water resources*.
907 volume 323. US Geological Survey Reston, VA.
- 908 Hibbard, K.A., Law, B.E., Reichstein, M., Sulzman, J., 2005. An analy-
909 sis of soil respiration across northern hemisphere temperate ecosystems.
910 *Biogeochemistry* 73, 29–70.
- 911 Jeannin, P.Y., Malard, A., Häuselmann, P., 2017. Effect of cave ventilation on
912 karst water chemographs, in: Renard, P., Bertrand, C. (Eds.), *Eurokarst*
913 2016, Springer, Neuchâtel, Switzerland. pp. 129–139.
- 914 Johnson, M., Billett, M., Dinsmore, K., Wallin, M., Dyson, K., Jassal, R.,
915 2010. Direct and continuous measurement of dissolved carbon dioxide in
916 freshwater aquatic systems - method and applications. *Ecohydrology* 3,
917 68–78.
- 918 Knierim, K., Pollock, E., Hays, P., Khojasteh, J., 2015a. Using Stable Iso-
919 topes of Carbon to Investigate the Seasonal Variation of Carbon Transfer
920 in a North-western Arkansas Cave. *Journal of Cave and Karst Studies* 77,
921 12–27.
- 922 Knierim, K.J., Hays, P.D., Bowman, D., 2015b. Quantifying the variability in
923 *Escherichia coli* throughout storm events at a karst spring in northwestern
924 Arkansas, United States. *Environmental Earth Sciences* 74, 4607–4623.

- 925 Knierim, K.J., Pollock, E.D., Covington, M.D., Hays, P.D., Brye, K.R., 2017.
926 Carbon cycling in the mantled karst of the Ozark Plateaus, central United
927 States. *Geoderma Regional* 10, 64–76.
- 928 Larock, B.E., Jeppson, R.W., Watters, G.Z., 2000. *Hydraulics of pipeline*
929 *systems*. CRC Press.
- 930 Lloyd, J., Taylor, J.A., 1994. On the Temperature Dependence of Soil Res-
931 piration. *Functional Ecology* 8, 315.
- 932 Luetscher, M., Jeannin, P.Y., 2004. Temperature distribution in karst sys-
933 tems: the role of air and water fluxes. *Terra Nova* 16, 344–350.
- 934 Luetscher, M., Lismonde, B., Jeannin, P.Y., 2008. Heat exchanges in the
935 heterothermic zone of a karst system: Monlesi cave, Swiss Jura Mountains.
936 *Journal of Geophysical Research: Earth Surface* 113, 1–13.
- 937 Matthey, D.P., Atkinson, T.C., Barker, J.A., Fisher, R., Latin, J.P., Durrell,
938 R., Ainsworth, M., 2016. Carbon dioxide, ground air and carbon cycling
939 in Gibraltar karst. *Geochimica et Cosmochimica Acta* 184, 88–113.
- 940 McFarland, J.D., 1998. *Stratigraphic summary of Arkansas*. volume 36.
941 *Arkansas Geological Commission*.
- 942 Palmer, A., 2007a. *Cave Geology*. Cave Books, Dayton, OH.
- 943 Palmer, A.N., 1991. Origin and morphology of limestone caves. *Bull. Geol.*
944 *Soc. Am.* 103, 1–21.
- 945 Palmer, A.N., 2007b. Variation in rates of karst processes. *Acta Carsologica*
946 36, 15–24.
- 947 Plummer, L., Wigley, T., Parkhurst, D.L., 1978. The Kinetics of Calcite
948 Dissolution in CO₂-Water Systems at 5° to 60° C and 0.0 to 1.0 ATM
949 CO₂. *American Journal of Science* 278, 179–216.
- 950 Pugh, A.L., Westerman, D.A., 2014. Mean annual, seasonal, and monthly
951 precipitation and runoff in Arkansas, 1951-2011. *USGS Scientific Investi-*
952 *gations Report* 5006.
- 953 Scanlon, B., Thraikill, J., 1987. Chemical similarities among physically
954 distinct spring types in a karst terrain. *Journal of Hydrology* 89, 259–279.

- 955 Schmidt, K.H., 1985. Regional variation of mechanical and chemical denuda-
956 tion, upper Colorado River Basin, U.S.A. *Earth Surface Processes and*
957 *Landforms* 10, 497–508.
- 958 Simms, M.J., 2004. Tortoises and hares: dissolution, erosion and isostasy in
959 landscape evolution. *Earth Surface Processes and Landforms* 29, 477–494.
- 960 Smith, D.L., Johnson, L., 2004. Vegetation-mediated changes in microclimate
961 reduce soil respiration as woodlands expand into grasslands. *Ecology* 85,
962 3348–3361.
- 963 Spötl, C., Fairchild, I.J., Tooth, A.F., 2005. Cave air control on dripwater
964 geochemistry, Obir Caves (Austria): Implications for speleothem deposi-
965 tion in dynamically ventilated caves. *Geochimica et Cosmochimica Acta*
966 69, 2451–2468.
- 967 Troester, J., White, W.B., 1984. Seasonal fluctuations in the carbon dioxide
968 partial pressure in a cave atmosphere. *Water Resources Research* 20, 153–
969 156.
- 970 U.S. Geological Survey, 2020. USGS water data for the Nation: U.S. Geo-
971 logical Survey National Water Information System database.
- 972 Whipple, K.X., Hancock, G.S., Anderson, R.S., 2000. River incision into
973 bedrock: Mechanics and relative efficacy of plucking, abrasion, and cavi-
974 tation. *Geological Society of America Bulletin* 112, 490–503.
- 975 Wigley, T., Brown, M., 1976. The Physics of Caves, in: Ford, T., Cullingford,
976 C. (Eds.), *The Science of Speleology*. Academic Press, New York, pp. 329–
977 358.
- 978 Wolman, M.G., Miller, J.P., 1960. Magnitude and frequency of forces in
979 geomorphic processes. *The Journal of Geology* 68, 54–74.
- 980 Wong, C.I., Banner, J.L., Musgrove, M., 2011. Seasonal dripwater Mg / Ca
981 and Sr / Ca variations driven by cave ventilation : Implications for and
982 modeling of speleothem paleoclimate records. *Geochimica et Cosmochim-*
983 *ica Acta* 75, 3514–3529.
- 984 Wood, W.W., 1985. Origin of caves and other solution openings in the un-
985 saturated (vadose) zone of carbonate rocks : A model for CO₂ generation.
986 *Geology* 13, 822–824.

- 987 Wood, W.W., Petraitis, M., 1984. Origin and Distribution of Carbon Dioxide
988 in the Unsaturated Zone of the Southern High Plains of Texas. *Water*
989 *Resources Research* 20, 1193–1208.
- 990 Worthington, S., Davies, G., Quinlan, J., 1992. Geochemistry of springs in
991 temperate carbonate aquifers: recharge type explains most of the varia-
992 tion, in: *Proceedings, Colloque d'Hydrologie en Pays Calcaire et en Milieu*
993 *Fissuré* (5th Neuchâtel, Switzerland). *Annales Scientifique de l'Université*
994 *de Bescancxon, Geologie-Mémoires Hors Série*, pp. 341–347.
- 995 Young, H., 2018. *Quantifying Carbon Dioxide Fluxes in the Air and Water*
996 *in Blowing Springs Cave, Arkansas*. M.S.. University of Arkansas. United
997 States – Arkansas.